Journal of Computational Chemistry & Molecular Modeling (ISSN: 2473-6260)

In silico Design of Novel N-hydrosulfonylbenzamides inhibitors of dengue RNA-dependent RNA polymerase showing favorable predicted pharmacokinetic profiles

DOI: 10.25177/JCCMM.5.2.RA.10756

Research

Accepted Date: 25th August 2021; Published Date:30th August 2021

Kouakou Kouakou Jean-Louis [1], Melalie Keita [1*], Akori Elvice Esmel [1], Brice Dali [1], Aubin N'Guessan [1], Affiba Florance Kouassi [1]

[1] Laboratoire de Physique Fondamentale et Appliquée (LPFA), University of Abobo Adjamé (now Nangui Abrogoua), Abidjan, Côte d'Ivoire;

Author Email ID: louisetjojo@yahoo.fr, keitamelalie@yahoo.fr, elvicee@yahoo.fr, dalibrice@yahoo.fr, nguessaubin@gmail.com, akouassi859@yahoo.com

CORRESPONDENCE AUTHOR
Melalie Keita
Email ID: keitamelalie@yahoo.fr;
Tel.: +225-07-07-82-93-40

CITATION
Melalie Keita, Kouakou Kouakou Jean-Louis, Akori Elvice Esmel, Brice Dali, Aubin N'Guessan, Affiba Florance Kouassi, In silico Design of Novel N-hydrosulfonylbenzamides inhibitors of dengue RNA-dependent RNA polymerase showing favorable predicted pharmacokinetic profiles(2021) Journal of Computational Chemistry & Molecular Modeling 5(2) p:561-584

ABSTRACT

Background: In recent years, there has been a growing interest in Denv NS5 inhibition, with several reported RdRp inhibitors such as sulfonylbenzamides, non-nucleo-side inhibitors without any 3D-QSAR pharmacophore (PH4) available. In this context, we report here, *in silico* design and virtual evaluation of novel sulfonylbenzamides Denv RdRp inhibitors with favorable predicted pharmacokinetic profile.

Methods: By using *in situ* modifications of the crystal structure of 5-(5-(3-hydroxyprop-1-yn-1-yl)thiophen-2-yl)-4- methoxy-2-methyl-N-(methylsulfonyl) benzamide (EHB)-RdRp complex (PDB entry 5HMZ), 3D models of RdRp-EHB$_x$ complexes were prepared for a training set of 18 EHBs with experimentally determined inhibitory potencies (half-maximal inhibitory concentrations IC_{50}^{exp}). In the search for active conformation of the EHB1-18, linear QSAR model was prepared, which correlated computed gas phase enthalpies of formation $(\Delta\Delta H_{MM})$ of RdRp-EHB$_x$ complexes with the IC_{50}^{exp}. Further, considering the solvent effect and entropy changes upon ligand binding resulted in a superior QSAR model correlating computed complexation Gibbs free energies $(\Delta\Delta G_{com})$. The successive pharmacophore model (PH4) generated from the active conformations of EHBs served as a virtual screening tool of novel analogs included in a virtual combinatorial library (VCL) of compounds with scaffolds restricted to phenyl. The VCL filtered by the Lipinski's rule-of-five was screened by the PH4 model to identify new EHB analogs.

Results: Gas phase QSAR model: $-\log_{10}(IC_{50}^{exp}) = pIC_{50}^{exp} = -0.1403 \times \Delta\Delta H_{MM} + 7.0879$, $R^2 = 0.73$; superior aqueous phase QSAR model: $pIC_{50}^{exp} = -0.2036 \times \Delta\Delta G_{com} + 7.4974$, $R^2 = 0.81$ and PH4 pharmacophore model: $pIC_{50}^{exp} = 1.0001 \times pIC_{50}^{pre} - 0.0017$, $R^2 = 0.97$. The VCL of more than 30 million EHBs was filtered down to 125,915 analogs Lipinski's rule. The five-point PH4 screening retained 329 new and potent EHBs with predicted inhibitory potencies IC_{50}^{pre} up to 30 times lower than that of EHB1 $(IC_{50}^{exp} = 23\ nM)$. Predicted pharmacokinetic profile of the new analogs showed enhanced cell membrane permeability and high human oral absorption compared to the alone drug to treat dengue virus.

Conclusions: Combined use of QSAR models, which considered binding of the EHBs to RdRp, pharmacophore model and ADME properties helped to recognize bound active conformation of the sulfonylbenzamide inhibitors, permitted *in silico* screening of VCL of compounds sharing sulfonylbenzamide scaffold and identify new analogs with predicted high inhibitory potencies and favorable pharmacokinetic profiles.

Keywords: ADME properties prediction, Dengue, 3-(5-ethynylthiophen-2-yl)-N-hydrosulfonylbenzamides, in *silico* screening, RNA-dependent RNA polymerase.

1. INTRODUCTION

Emerging" and / or "re-emerging" diseases have been public health deep concern in recent decades. The incidence of dengue fever is currently increasing dramatically and is now included among the so-called "re-emerging" diseases. The World Health Organization (WHO) estimates the number of annual cases at 50 million, including 500,000 cases of dengue haemorrhagic fever which are fatal in more than 20% of cases [1]. According to data received from the Early Warning System, part of the WHO Public Health Case Management System - Event Management System (EMS) - 52 public health cases have been reported to the WHO Regional Office for Africa between January and September 2014, of which 94% (49/52) were due to infectious diseases; dengue (11%) after cholera (33%) [1].

Currently no specific medicine against dengue fever and the only approved vaccine, Dengvaxia®, developed by Sanofi Pasteur [2] is contraindicated to children under 9 and in adults over 45 years old. According to the WHO Dengvaxia® Vaccine Report (September 2018), the live attenuated dengue vaccine CYD-TDV has been shown to be effective and safe in clinical trials in people who previously had an infection with the dengue virus (HIV positive people). However, it carries an increased risk of severe dengue fever in those who experience their first natural dengue infection after vaccination (those who were HIV negative at the time of vaccination).

Dengue fever causative agents are four dengue viruses (Denv 1, Denv 2, Denv 3 and Denv 4). Dengue virus contains an 11 kb positive-sense, single-stranded RNA genome. The genome consists of a single open reading frame which encodes three structural proteins (capsid C, premembrane/membrane (prM/M), and envelope (E) protein), and seven non-structural proteins (NS1, NS2A, NS2B, NS3, NS4A, NS4B, and NS5) [3]. The structural proteins form the viral particle and the non-structural proteins participate in the replication of the RNA genome, virion assembly and invasion of innate immune response [4]. NS5 is the most conserved protein of the dengue proteome as it shares a minimum of 67% amino acid sequence across all four dengue serotypes [5,6]. NS5 is essential for RNA replication and performs enzymatic activities required for capping and synthesis of RNA genome of virus. It consists of two domains with distinct functions, the N-terminal methyl transferase (MTase) and the C-terminal RNA-dependent RNA polymerase (RdRp) catalytic domain [6,7]. The tertiary structure of RdRp consists of palm thumb and finger subdomains. The catalytic site contains conserved aspartic residues.

In recent years, there has been a growing interest in Denv NS5, with several groups reporting RdRp inhibitors [8,9,10,11,12,13,14,15]. A series of NS5 RdRp inhibitors recently has been reported which has led to the identification of 5-(5-(3-Hydroxyprop-1-yn-1-yl)thiophen-2-yl)-2,4-dimethoxy-N-((3-methoxyphenyl)sulfonyl)benzamide ($IC_{50}^{exp} = 170$ nM 27) and 5-(5-(3-Hydroxyprop-1-yn-1-yl) thiophen-2-yl)-4-methoxy-2-methyl-N-(quinolin-8-ylsulfonyl)benzamide ($IC_{50}^{exp} = 23$ nM 29) as promising avenues for further optimization and development [16]. The 3D-QSAR pharmacophores (PH4) for RdRp inhibition are not available so far, to our knowledge for these inhibitors.

The main objective of this work was to design novel potent 3-(5-ethynylthiophen-2-yl)-N-hydrosulfonylbenzamides (EHBs) based on a series of 18 (training set) and 4 (validation set) nanomolar inhibitors with observed inhibitory potencies as high as $IC_{50}^{exp} = 23$ nM [16]. Starting through *in situ* modification of the crystal structure of RdRp-EHB5 complex (PDB: 5HMZ) we have elaborated a QSAR model which correlated Gibbs free energies of RdRp-EHBx complex formation with the potencies IC_{50}^{exp} and determined the active conformation of EHBs bound at the active site of RdRp of Denv (MM-PB complexation approach). Based on this active conformation we have formulated 3D QSAR pharmacophore of RdRp inhibition (PH4). Large virtual library of compounds sharing the EHB scaffold has been generated and in *silico* screened with the PH4. The screening yielded virtual hits that exhibited predicted inhibitory potencies IC_{50}^{pre} more than 30 times higher than the most active training set compound EHB1. Several of the identified putative inhibitors displayed favorable ADME profiles.

2. MATERIALS & METHODS

2.1. Training and validation sets

Chemical structures and biological activities (IC_{50}^{exp}) of training and validation sets of *3-(5-ethynylthiophen-2-yl)-N-hydrosulfonylbenzamides* inhibitors of RdRp used in this study were taken from literature [16]. The potencies of these compounds cover a sufficiently broad range of half-maximal inhibitory concentrations ($23 \leq IC_{50}^{exp} \leq 734{,}000$ nM) to allow construction of a QSAR model. The training set (TS) containing 18 EHB inhibitors and the validation set (VS) including 4 EHV were taken from the ref. [16].

2.2. Model building

Three dimensional (3D) molecular models of enzyme-inhibitor (E-I) complexes *RdRp*-EHBx, free enzyme RdRp and free inhibitors EHBx were prepared from high-resolution (1.99 Å) crystal structure of a reference complex containing the training set compound 5-(5-(3-hydroxyprop-1-yn-1-yl)thiophen-2-yl)-4-methoxy-2-methyl-N-(methylsulfonyl)benzamide (EHB5, Table 1) bound to the RdRp (Protein Data Bank [29] entry code 5HMZ [16]) using Insight-II molecular modeling program [30].

The structures of RdRp and the E-I complexes were at pH of 7 with neutral N- and C-terminal residues and all protonizable and ionizable residues charged. No crystallographic water molecules were included into the model. The inhibitors were built into the reference structure 5HMZ [16] by *in situ* replacing of derivatized groups in the molecular scaffold of the template inhibitor EHB5. An exhaustive conformational search over all rotatable bonds of the replacing function groups coupled with a careful gradual energy-minimization of the modified inhibitor and active site residues of the RdRp located in the vicinity of the inhibitor (within 5Å distance), was employed to identify low-energy bound conformations of the modified inhibitor. The resulting low-energy structures of the E-I complexes were then carefully refined by minimization of the whole complex. This procedure has been successfully used for model building of viral, bacterial and protozoal enzyme-inhibitor complexes and design of peptidomimetic, hydroxynaphthoic, thymidine, triclosan, pyrrolidine carboxamide, nitriles and chalcone-based inhibitors [22, 31, 32, 33, 34, 35, 36, 37, 38, 39, 40].

2.3. Molecular mechanics

Modeling of inhibitors, RdRp and E-I complexes was carried out by molecular mechanics as described earlier [22].

2.4. Conformational search

Free inhibitor conformations were derived from their bound conformations in the E-I complexes by gradual relaxation to the nearest local energy minimum as described earlier [22].

2.5 Solvation Gibbs free energies

The electrostatic component of solvation Gibbs free energy (GFE) that includes also the effects of ionic strength via solving nonlinear Poisson–Boltzmann equation [41,42] was computed by the Delphi module in Discovery Studio [20] as described earlier [22].

2.6 Calculation of Binding affinity and QSAR Model

The calculation of binding affinity expressed as complexation GFE has been described fully earlier [22].

2.7 Interaction Energy

The calculation of MM interaction energy (E_{int}) between enzyme residues and the inhibitor CFF91 force field [42] was performed as described earlier [22].

2.8. Pharmacophore Generation

Bound conformations of inhibitors taken from the models of E-I complexes were used for constructing of 3D-QSAR pharmacophore (PH4) by means of Catalyst HypoGen algorithm [43] implemented in Discovery Studio [20] as described earlier [22].

2.9. ADME Properties

The pharmacokinetics profile of EHBs were computed by the QikProp program [26] as described earlier [22].

2.10. Virtual Library Generation

The virtual library generation was performed as described earlier [22].

2.11. ADME-Based Library Searching

The drug-likeness selection criterion served to focus the initial virtual library as described earlier [22].

2.12. Pharmacophore-Based Library Searching

The pharmacophore model (PH4) described in Section 4.8 and derived from the bound conformations of EHBs at the active site of RdRp served as library searching tool as described earlier [22].

2.13. Inhibitory Potency Prediction

The conformer with the best mapping on the PH4 pharmacophore in each cluster of the focused library subset was used for $\Delta\Delta G_{com}$ calculation and IC_{50}^{pre} estimation (virtual screening) by the complexation QSAR model as described earlier [22].

3. RESULTS

3.1 Training and Validation Sets

The training set of 18 EHB and validation set of 4 analogs (Table 1) were selected from a series of NS5 RdRp inhibitors with known experimentally determined inhibitory activities. The whole series was obtained by substitution at five positions R_1, R_2, R_3, R_4, and R_5 of the phenyl ring and R group as shown in Table 1. The experimental half-maximal inhibitory concentrations $(23 \leq IC_{50}^{exp} \leq 734{,}000\ nM)$ [16] cover a sufficiently wide concentration range for building of a reliable QSAR model.

Table 1. Set (EHB1-18) and validation set (EHV1-4) of NS5 RdRp inhibitors [16] used in the preparation of QSAR models of inhibitor binding. The R groups are numbered as #R ≡ group index.

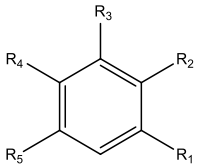

#R	1	2	3	4	5	6	7
R-group		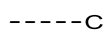	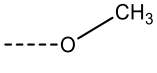	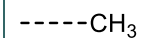	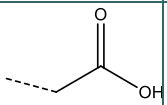	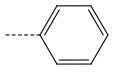	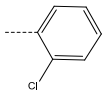

#R	8	9	10	11	12	13	14
R-group	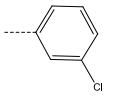	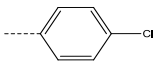	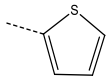	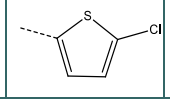	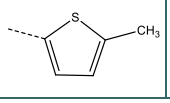	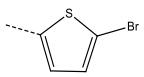	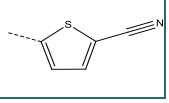

#R	15	16	17	18	19	20	21
R-group	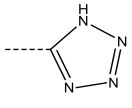	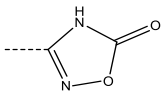	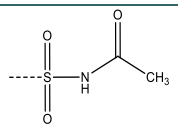	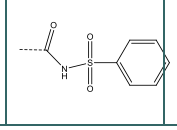	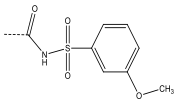	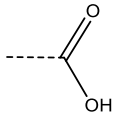	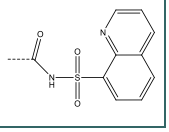

#R	22	23
R-group	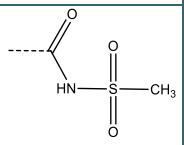	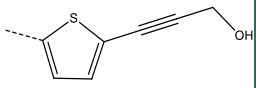

Training Set	EHB1	EHB2	EHB3	EHB4	EHB5	EHB6	EHB7
R_1-R_2-R_3-R_4-R_5	23-3-1-4-21	23-2-1-3-19	23-3-1-3-19	23-3-1-3-18	23-3-1-4-22	23-3-1-1-15	23-3-1-4-17
IC_{50}^{exp} (nM)	23	140	170	250	340	2400	2500

Training Set	EHB8	EHB9	EHB10	EHB11	EHB12	EHB13	EHB14
R_1-R_2-R_3-R_4-R_5	23-3-1-4-16	23-3-1-1-5	10-1-5-1-5	11-1-5-1-5	13-1-5-1-5	9-1-5-1-5	12-1-5-1-5
IC_{50}^{exp} (nM)	3200	7500	15,000	26,000	39,000	62,000	96,000

Training Set	EHB15	EHB16	EHB17	EHB18
R_1-R_2-R_3-R_4-R_5	8-1-5-1-5	7-1-5-1-5	14-1-5-1-5	6-3-1-1-5
IC_{50}^{exp} (nM)	141,000	192,000	199,000	734,000

Validation Set	EHV1	EHV2	EHV3	EHV4
R_1-R_2-R_3-R_4-R_5	23-3-1-4-18	23-3-1-4-20	23-3-1-1-20	6-1-5-1-5
IC_{50}^{exp} (nM)	170	530	2300	177,000

3.2 QSAR Model

3.2.1 One Descriptor QSAR Models

Each of the 18 training sets (TS) and 4 validation sets (VS) RdRp-EHBx complexes (Table 1), was prepared by *in situ* modification of the refined template crystal structure (PDB entry code 5HMZ [16]) of the complex RdRp-EHB5 as described in the Methods section. Further, the relative Gibbs free energy of the RdRp-EHBx upon complex formation ($\Delta\Delta G_{com}$) was computed for each of the 22 optimized enzyme–inhibitor complexes. Table 2 lists computed values of $\Delta\Delta G_{com}$ and its components for the TS and VS of sulfonylbenzamides [16]. The QSAR model explained variation in the EHBs experimental inhibitory potencies ($pIC_{50}^{exp} = -\log_{10}(IC_{50}^{exp})$) [16]) by correlating it with computed GFE $\Delta\Delta G_{com}$ through a linear regression. In addition, significant correlation obtained in this QSAR relationship permitted to determine the active bound conformation of the EHBs at the RdRp binding site and enabled generation of the Denv RdRp inhibition PH4 pharmacophore. In search for a better insight into the binding affinity of EHBs towards Denv RdRp, we have analyzed the enthalpy of complexation in gas phase $\Delta\Delta H_{MM}$ by correlating it with the pIC_{50}^{exp}. The validity of this linear correlation (for statistical data of the regression see Table 3, Equation A) allowed assessment of the significance of inhibitor-enzyme interactions ($\Delta\Delta H_{MM}$) when solvent effect and loss of entropy of the inhibitor upon binding to the enzyme were neglected. This in extremis and unexpected correlation due to the non-homogeneity of molecules explained about 73% of the pIC_{50}^{exp} data variation and underlined the role of the enthalpic contribution to the binding affinity of the ligand. More, the advanced descriptor, namely the GFE of the RdRp-EHBx complex formation including all components: $\Delta\Delta H_{MM}$, $\Delta\Delta TS_{vib}$ and $\Delta\Delta G_{sol}$, has been assessed (for statistical data see Table 3, Equation B). Relatively high values of the regression coefficient R^2, leave-one-out cross-validated regression coefficient R_{xv}^2 and Fischer F-test of the correlation show the importance of the term entropic in the biological environment and suggest a good relationship between the 3D model of inhibitor binding and the observed inhibitory potencies of the EHBx [16] .Therefore, structural information derived from the 3D models of RdRp – EHBx complexes is expected to lead to reliable prediction of RdRp inhibitory potencies for novel EHBs analogs based on the QSAR model B, Table 3.

Table 2. Gibbs free energy (binding affinity) and its components for the training set of RdRp inhibitors EHB1-18 and validation set inhibitors EHV1-4 [16].

Training Set [a]	M_W [b] $g.mol^{-1}$	$\Delta\Delta H_{MM}$ [c] $kcal.mol^{-1}$	$\Delta\Delta G_{sol}$ [d] $kcal.mol^{-1}$	$\Delta\Delta TS_{vib}$ [e] $kcal.mol^{-1}$	$\Delta\Delta G_{com}$ [f] $kcal.mol^{-1}$	IC_{50}^{exp} [g] nM
EHB1	492	0	0	0	0	23
EHB2	491	8.37	-1.77	-2.09	8.68	140
EHB3	487	5.43	-2.33	0.31	2.79	170
EHB4	457	0.55	8.24	0.05	8.75	250
EHB5	379	7.99	-2.38	-0.20	5.81	340
EHB6	312	15.14	-6.07	-1.15	10.22	2400
EHB7	379	7.55	4.62	1.65	10.52	2500
EHB8	342	12.24	-6.36	-0.83	6.71	3200
EHB9	302	14.61	-7.62	-1.94	8.93	7500
EHB10	276	22.11	-8.70	1.06	12.35	15,000
EHB11	310	19.59	-4.54	-1.51	16.56	26,000
EHB12	353	21.07	-4.79	-1.50	17.79	39,000
EHB13	304	13.12	-1.95	-1.21	12.38	62,000
EHB14	290	22.14	-5.99	-2.28	18.43	96,000
EHB15	304	13.05	-1.91	-1.94	13.08	141,000
EHB16	304	15.68	-1.87	-1.66	15.46	192,000
EHB17	301	20.72	-5.44	-1.95	17.24	199,000
EHB18	228	29.72	-6.11	1.42	22.19	734,000
Validation Set [a]	**M_W [b] $g.mol^{-1}$**	**$\Delta\Delta H_{MM}$ [c] $kcal.mol^{-1}$**	**$\Delta\Delta G_{sol}$ [d] $kcal.mol^{-1}$**	**$\Delta\Delta TS_{vib}$ [e] $kcal.mol^{-1}$**	**$\Delta\Delta G_{com}$ [f] $kcal.mol^{-1}$**	**$pIC_{50}^{pre}/pIC_{50}^{exp}$ [h]**
EHV1	441	7.09	-3.4	0.07	3.63	1.00
EHV2	302	10.66	-4.63	-0.33	6.35	0.87
EHV3	288	11.39	-5.50	-1.79	7.67	0.92
EHV4	270	8.92	1.71	-0.07	10.71	1.22

[a] for the chemical structures of the training set of inhibitors see Table 1.

[b] M_W is the molar mass of inhibitors.

[c] $\Delta\Delta H_{MM}$ is the relative enthalpic contribution to the Gibbs free energy change related to E:I complex formation derived by molecular mechanics (MM): $\Delta\Delta H_{MM} \cong [E_{MM}\{E{:}I_x\} - E_{MM}\{I_x\}] - [E_{MM}\{E{:}I_{ref}\} - E_{MM}\{I_{ref}\}]$, I_{ref} is the reference inhibitor EHB1;

[d] $\Delta\Delta G_{sol}$ is the relative solvation Gibbs free energy contribution to the Gibbs free energy change related to E:I complex formation: $\Delta\Delta G_{sol} = [G_{sol}\{E{:}I_x\} - G_{sol}\{I_x\}] - [G_{sol}\{E{:}I_{ref}\} - G_{sol}\{I_{ref}\}]$;

[e] $-\Delta\Delta TS_{vib}$ is the relative entropic contribution of the inhibitor to the Gibbs free energy related to E:I complex formation: $\Delta\Delta TS_{vib} = [\Delta\Delta TS_{vib}\{I_x\}_E - \Delta\Delta TS_{vib}\{I_x\}] - [\Delta\Delta TS_{vib}\{I_{ref}\}_E - \Delta\Delta TS_{vib}\{I_{ref}\}]$;

[f] $\Delta\Delta G_{com}$ is the relative Gibbs free energy change related to E:I complex formation: $\Delta\Delta G_{com} \cong \Delta\Delta H_{MM} + \Delta\Delta G_{sol} - \Delta\Delta TS_{vib}$.

[g] IC_{50}^{exp} is the experimental RdRp half maximal inhibition concentration obtained from reference [16].

[h] Ratio of predicted and experimental half maximal inhibition concentrations $pIC_{50}^{pre}/pIC_{50}^{exp}$. $pIC_{50}^{pre} = -\log_{10}(IC_{50}^{pre})$ was predicted from computed $\Delta\Delta G_{com}$ using the regression equation for RdRp shown in Table 3, B.

Table 3. Analysis of computed binding affinities $\Delta\Delta G_{com}$, its enthalpic component $\Delta\Delta H_{MM}$ and experimental half-maximal inhibitory concentrations $pIC_{50}^{exp} = -\log_{10}(IC_{50}^{exp})$ of EHBs towards Denv RdRp [16].

Statistical Data of linear Regression	**(A)**	**(B)**
$pIC_{50}^{exp} = -0.1403 \times \Delta\Delta H_{MM} + 7.0879$ (A)		
$pIC_{50}^{exp} = -0.2036 \times \Delta\Delta G_{com} + 7.4974$ (B)		
Number of compounds n	18	18
Squared correlation coefficient of regression R^2	0.73	0.81
LOO cross-validated squared correlation coefficient R^2_{xv}	0.71	0.80
Standard error regression σ	0.342	0.318
Statistical significance of regression, Fisher F-test	42.40	67.40
Level of statistical significance α	>95%	
Range of activities IC_{50}^{exp} [nM]	23 - 734000	

The statistical data confirmed validity of the correlation Equations (A) and (B) plotted on Figure 1. The ratio $pIC_{50}^{pre}/pIC_{50}^{exp} \cong 1$ (the pIC_{50}^{pre} values were estimated using correlation Equation B, Table 3) calculated for the validation set EHV1-4 documents the substantial predictive power of the complexation QSAR model from Table 2. Thus, the regression Equation B (Table 3) and computed GFE $\Delta\Delta G_{com}$ can be used for prediction of inhibitory potencies IC_{50}^{pre} against Denv RdRp for novel EHB analogs provided they share the same binding mode as the training set sulfonylbenzamides EHB1-18.

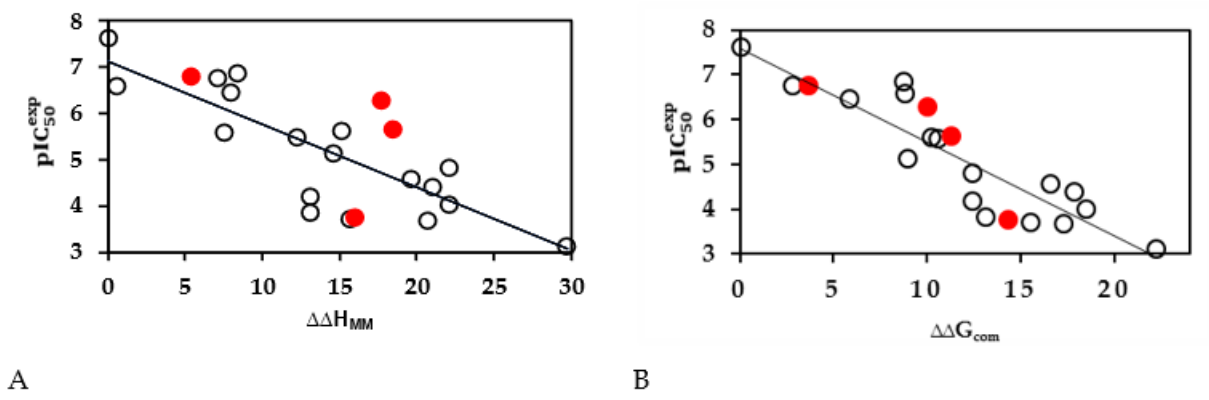

Figure 1. (A) Plot of correlation equation between pIC_{50}^{exp} and relative enthalpic contribution to the GFE $\Delta\Delta H_{MM}$ [kcal·mol^{-1}]. (B) Similar plot for relative complexation Gibbs free energies of the RdRp-EHBx complex formation $\Delta\Delta G_{com}$ [kcal·mol^{-1}] of the training set [16]. The validation set data points are shown in red color.

3.2.2 Binding Mode of EHBs

The 3D crystal structure of Denv RdRp adopts a classical polymerase hand shape with fingers, palm, and thumb subdomains [17]. This last part contains the initiation loop which triggers the polymerization process of the viral RNA close to the palm with the catalytic residues ASP 663 and ASP 664 [6,18,19]. The recently reported x-rays complex of Denv RdRp and non-nucleoside inhibitors reveals that the propargyl alcohol projected into the narrow cavity and formed two Hbond interactions with His 800 and Glu 802. The sulfonylbenzamide is involved in three Hbond contacts with the side chains of Thr 794 and Arg 729 and the backbone of Trp 795. Changes made to this methyl have improved the activity but limited still to the two digits nanomolar range (IC_{50}^{exp} = 23 nM) [16].

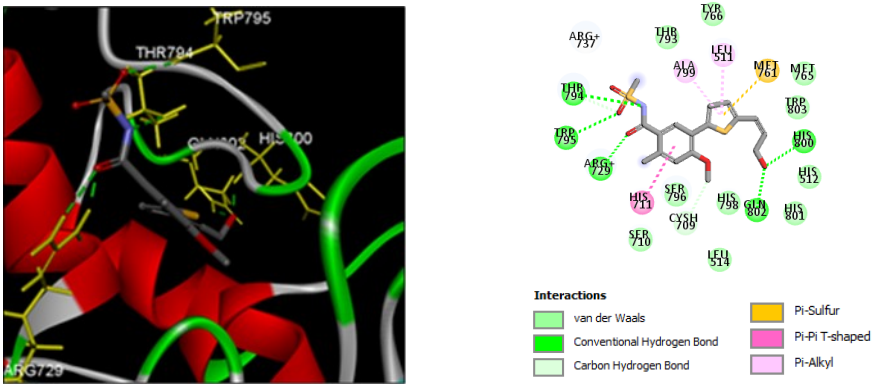

(A) **(B)**

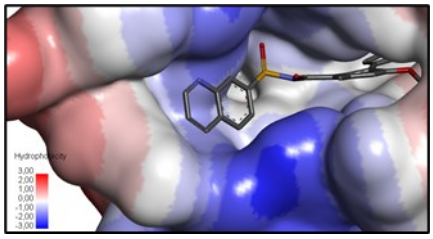

(C)

Figure 2. (A) 3D structure of the Denv RdRp active site with bound inhibitor EHB5 (5HMZ.pdb). (B) 2D schematic interaction diagram of the inhibitor EHB5 [16] at the active site of Denv RdRp. (C) Hydrophobic surface of the active site of Denv RdRp with the most potent inhibitor EHB1 [16]. Surface coloring legend: red = hydrophobic, blue = hydrophilic and white = intermediate.

3.3. Interaction Energy

Other key structural information was provided by the interaction energy (IE, ΔE_{int}) diagram obtained for each training set inhibitor. IE breakdown to contributions from Denv RdRp active site residue helpfully directs the choice of relevant R-groups able to improve the binding affinity of EHB analogs to the Denv RdRp and subsequently enhance the inhibitory potency. A comparative analysis of computed IE for training set EHBx (Figure 4) divided into three classes (highest: 23 – 340 nM, moderate: 2400 – 7500 nM, and lowest activity: 26,000 – 734,000 nM) has been carried out to identify the residues for which the contribution to binding affinity could be increased. The comparative analysis showed IE contributions of active site residues for the three classes of inhibitors that should be retained or even improved such as those of Leu 511, His 711, Arg 737 and Thr 794. However, interactions with residues such as Met 340, Glu 733 Met 765 and Gln 802 are accentuated from the low activity class to the high activity class via that of medium activity. It should be noted that these residues Met 340, Glu 733 and Met 765 had not been listed as belonging to the active site (PDB:5HMZ) [16]. Since specific substitutions could not be proposed, we have adopted a combinatorial approach to novel EHB analogs design and in *silico* screened a virtual library of EHB analogs with help of the PH4 pharmacophore of Denv RdRp inhibition derived from the complexation QSAR model.

The statistical data confirmed validity of the correlation Equation plotted on Figure 3. This correlation of 88 % shows that there are interactions to be made to maintain or improve the activity of the new analogs.

Table 4. Analysis of computed binding affinities $\Delta\Delta E_{int}$ and experimental half-maximal inhibitory concentrations $pIC_{50}^{exp} = -\log_{10}(IC_{50}^{exp})$ of EHBx towards Denv RdRp [16].

Statistical Data of Linear Regression $pIC_{50}^{exp} = -0.1046 \times \Delta\Delta E_{int} + 7.2310$	
Number of compounds n	18
Squared correlation coefficient of regression R^2	0.88
Cross-validated squared correlation coefficient R^2_{xv}	0.87
Standard error of regression σ	0.225
Statistical significance of regression, Fisher F-test	113.58
Level of statistical significance α	>95%
Range of experimental activity IC_{50}^{exp} [nM]	23 - 734000

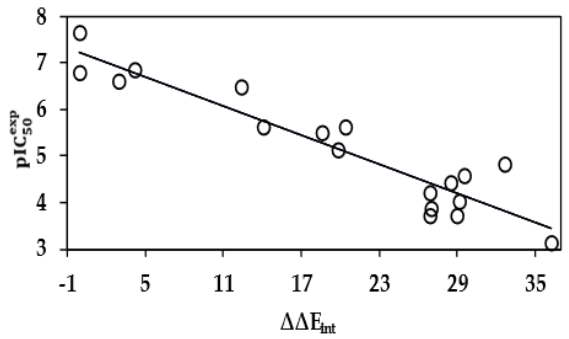

Figure 3. Plot of correlation equation between pIC_{50}^{exp} and relative interaction energies on the active site of the RdRp-EHBx complex.

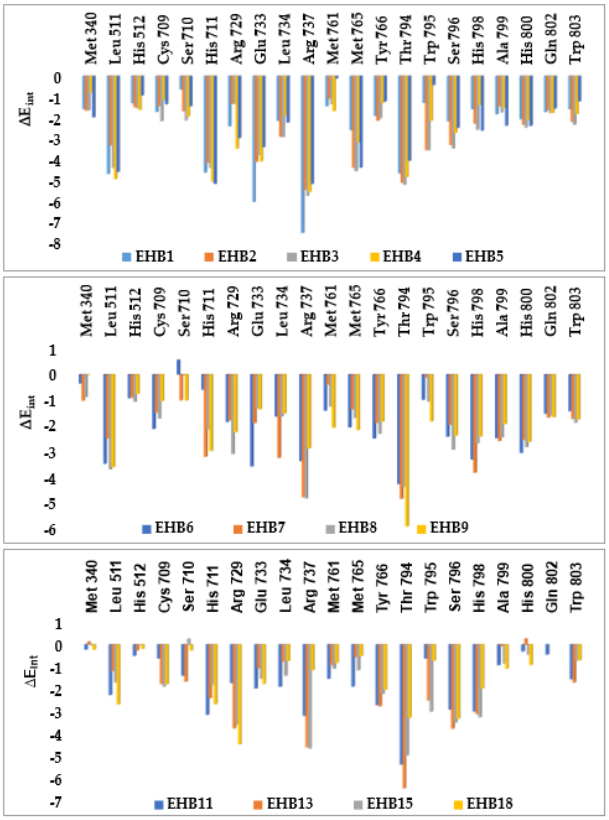

Figure 4. Mechanics intermolecular interaction energy E_{int} breakdown to residue contributions in [$kcal.mol^{-1}$]: (A) the most active inhibitors EHB1-5, (B) moderately active inhibitors EHB6-9, (C) a few of less active inhibitors EHB10 -18, Table 2 [16].

3.4. 3D-QSAR Pharmacophore Model

RdRp inhibition 3D-QSAR pharmacophore was generated from the active conformation of 18 TS EHB1-18 and evaluated by 4 VS EHV1-4 covering a large range of experimental activity (23 - 734000 nM) spanning more than two orders of magnitude. The generation process is divided into three main steps: (i) the constructive step, (ii) the subtractive step, and (iii) the optimization step [20]. During the constructive phase, EHB1 alone was retained as the lead (since only the activity of EHB1 fulfilled the threshold criterion: $IC_{50}^{exp} \leq 1.25 \times 23$ nM) and used to generate the starting PH4 features. In the subtractive phase, compounds for which: $IC_{50}^{exp} > 23 \times 10^{3.5}$ nM = 72,732 nM were considered inactive. As a result, EHB14, EHB15, EHB16, EHB17 and EHB18 from the EHBx training set were inactive. Finally, during the optimization phase, the score for pharmacophoric hypotheses was improved. The assumptions were scored based on errors in the regression activity and complexity estimates via a simulated annealing approach. At the end of the optimization, the 10 highest-rated unique pharmacophore hypotheses were retained, all showing five-point characteristics. The cost values, correlation coefficients, root mean square deviation (RMSD) values, pharmacophore characteristics and max-fit value of the first 10 ranked hypotheses (Hypo1 - Hypo10) are listed in Table 5. They were selected based on statistically significant parameters, such as high correlation coefficient, low total cost and low RMSD.

Table 5. Parameters of 10 generated PH4 pharmacophoric hypotheses for RdRp inhibitors after CatScramble validation procedure (49 scrambled runs for each hypothesis at the selected level of confidence of 98%).

Hypothesis	RMSD [a]	R^2 [b]	Total Cost [c]	Costs Difference [d]	Closest Random [e]
Hypo1	2.31	0.984	93.16	1 490.04	538.361
Hypo2	2.77	0.977	114.45	1 468.75	580.895
Hypo3	2.91	0.975	121.18	1 462.02	666.732
Hypo4	2.95	0.974	123.10	1 460.10	685.046
Hypo5	2.97	0.974	124.14	1 459.06	686.953
Hypo6	3.11	0.971	132.03	1 451.17	708.269
Hypo7	3.11	0.972	132.30	1 450.90	730.729
Hypo8	3.25	0.969	140.08	1 443.12	739.285
Hypo9	3.30	0.968	142.74	1 440.46	739.817
Hypo10	3.30	0.968	143.55	1 439.65	741.549

[a] Root Mean Square Deviation; [b] squared correlation coefficient; [c] overall cost parameter of the PH4 pharmacophore; [d] cost difference between Null cost and hypothesis total cost; [e] lowest cost from 49 scrambled runs at a selected level of confidence of 98%. The Fixed Cost = 44.55 with RMSD = 0, the Null Cost = 1583.2 with RMSD = 13.129 and the Configuration cost = 11.57.

The generated pharmacophore models were then assessed for their reliability based on the calculated cost parameters ranging from 93.16 (Hypo1) to 143.55 (Hypo10). The relatively small gap between the highest and lowest cost parameter corresponds well with the homogeneity of the generated hypotheses and consistency of the TS of EHBx. For this PH4 model, the fixed cost (44.55) is lower than the null cost (1583.2) by a difference $\Delta = 1\ 538.65$. This difference is a major quality indicator of the PH4 predictability ($\Delta > 70$ corresponds to an excellent chance or a probability higher than 90% that the model represents a true correlation [20]). To be statistically significant, a hypothesis must be as close as possible to the fixed cost and as far as possible from the null cost. For the set of 10 hypotheses, the difference $\Delta \geq 1\ 439.65$, which attests to the high quality of the pharmacophore model. The standard indicators such as the RMSD between the hypotheses ranged from 2.31 to 3.30, and the squared correlation coefficient (R^2) falls to an interval from 0.984 to 0.968. The first PH4 hypothesis with the closest cost (93.16) to the fixed one (44.55) and best RMSD and R^2 was retained for further analysis. The statistical data for the set of hypotheses (costs, RMSD, R^2) are listed in Table 5. The configuration cost (11.57 for all hypotheses) far below 17 confirms this pharmacophore as a reasonable one.

The link between the 98% significance and the number 49 scrambled runs of each hypothesis is based on the formula $S = [1 - (1 + X)/Y] \times 100$, with X the total number of hypotheses having a total cost lower than the original hypothesis (Hypo 1) and Y the total number of HypoGen runs (initial + random runs): $X = 0$ and $Y = (1 + 49)$, hence $98\% = \{1 - [(1 + 0)/(49 + 1)]\} \times 100$.

The evaluation of Hypo 1 was performed first through Fischer's randomization cross-validation test. The CatScramble program was used to randomize the experimental activities of the training set. At 98% confidence level, each of the 49 scramble runs created ten valid hypotheses, using the same features and parameters as in the generation of the original 10 pharmacophore hypotheses. Among them, the cost value of Hypo1 is the lowest compared with those of the 49 randomly generated hypotheses, as we can see in Table 5 where the lowest cost of the 49 random runs is listed for each original hypothesis, and none of them was as predictive as the original hypotheses generated shown in Table 5. Thus, there is a 98% probability that the best selected hypothesis Hypo1 represents a pharmacophore model for inhibitory activity of RdRp with a similar level of predictive power as the complexation QSAR model, which relies on the EHBx active conformation from 3D structures of the RdRp-EHBx complexes and computed GFE of enzyme–inhibitor binding $\Delta\Delta G_{com}$. Another evaluation of Hypo 1 is the mapping of the best active training set EHB1 (Figure 5) displaying the geometry of the Hypo1 pharmacophore of NS5RdRp inhibition. The regression equation for pIC_{50}^{exp} vs pIC_{50}^{pre} estimated from Hypo1: $pIC_{50}^{exp} = 1.0001 \times pIC_{50}^{pre} - 0.0017$ (n = 18, R^2= 0.969, $R^2_{xv} = 0.967$, F-test = 498.83, σ = 0,238, α > 98 %) is also plotted on Figure 5.

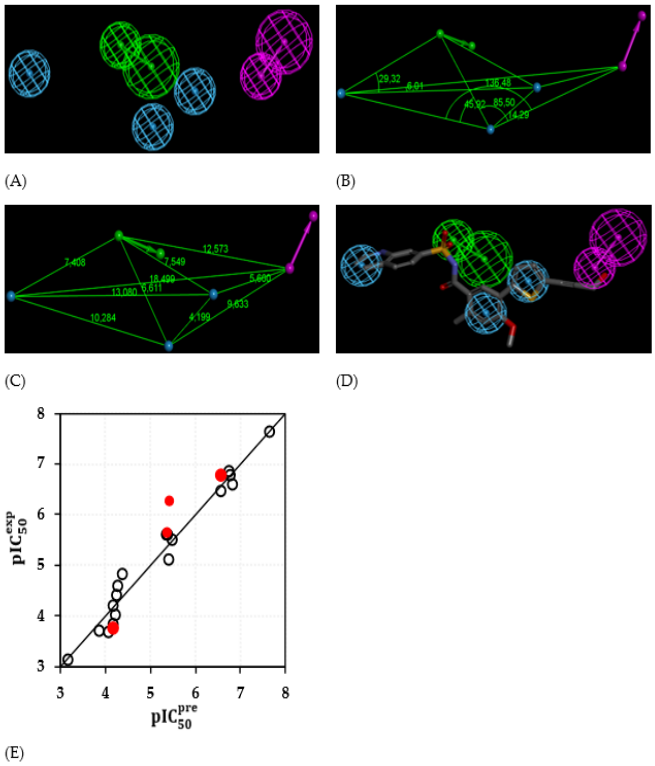

Figure 5. Features (A) coordinates of centers, (B) angles between centers of pharmacophoric features, (C) distances between centers, (D) mapping of pharmacophore of RdRp inhibitor with the most potent molecule EHB1. Features legend: HBD = Hydrogen bond Donor (magenta), HYDAr = Hydrophobic Aromatic (cyan), HBA = Hydrogen bond Acceptor (green). (E) Correlation plot of experimental vs. predicted inhibitory activity (open circles correspond to TS, red dots to VS).

We can carry out computational design and selection of new EHB analogs with elevated inhibitory potencies against Denv RdRp, based on a strategy using the noticeable presence of the hydrophobic features included in the best pharmacophore model at the position of R_5 coupled with mapping of R_1 to the HBD feature and the appropriate substitution to the others hydrophobic features in Hypo1 (Figure 5).

3.5. Virtual Screening

In *silico* screening of a virtual (combinatorial) library can lead to hit identification as it was shown in our previous works on inhibitors design [20,21,22].

3.5.1. Virtual Library

An initial virtual library (VL) was generated by substitutions at positions for R_1, R_2, R_3, R_4 and R_5 (see Table 6) on the phenyl ring scaffold. During the virtual library enumeration, the 221 R-groups listed in Table 6 were attached on following way: 1-7, 11, 18 to position R_1; 4, 8-20 to positions R_2 and R_3; 2, 4, 8-90 to position R_4 then all 221 R-groups to positions R_5 of the phenyl ring. The combinatorial library size is $R_1 \times R_2 \times R_3 \times R_4 \times R_5 = 9 \times 14 \times 14 \times 85 \times 221 = 33{,}136{,}740$ analogs. To design a more focused library of a reduced size and increased content of drug-like molecules, we have introduced a set of filters and penalties such as the Lipinski rule-of-five [23], which helped to select a smaller number of suitable EHBs that could be submitted to *in silico* screening. This focusing has reduced the size of the initial library to 125,915 analogs.

Table 6. R_1 to R_5-groups (fragments, building blocks, substituents) used in the design of the initial diversity virtual combinatorial library of sulfonylbenzamides.

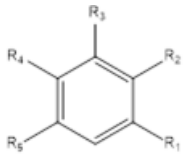

R-groups *					
1	5-(3-hydroxyprop-1-yn-1-yl)thiophen-2-yl	2	5-(3-aminoprop-1-yn-1-yl)thiophen-2-yl	3	5-(3-hydroxy-3-iminoprop-1-yn-1-yl)thiophen-2-yl
4	5-(mercaptoethynyl)thiophen-2-yl	5	5-(3-phosphinoprop-1-yn-1-yl)thiophen-2-yl	6	5-(hydrosulfonylEt)thiophen-2-yl
7	3-amino-3-oxoprop-1-yn-1-yl)thiophen-2-yl	8	MeO	9	Me
10	Cl	11	OH	12	ClMe
13	Methio	14	BrMe	15	Et
16	BrEt	17	H	18	NH_2
19	Meamino	20	Br	21	(butylsulfonyl)carbamoyl
22	(isopentylsulfonyl)carbamoyl	23	(S)-((3-Mepentyl)sulfonyl)carbamoyl	24	((3-Etpentyl)sulfonyl)carbamoyl
25	((cyclopropylMe)sulfonyl)carbamoyl	26	((cyclobutylMe)sulfonyl)carbamoyl	27	((cyclopentylMe)sulfonyl)carbamoyl
28	((cyclohexylMe)sulfonyl)carbamoyl	29	cycloprop-2-en-1-yl	30	thiophen-2-yl
31	thiophen-3-yl	32	5-Methiophen-2-yl	33	3,4,5-triMethiophen-2-yl
34	thiophen-2-ylMe	35	3-Methiophen-2-yl	36	3,5-diMethiophen-2-yl
37	((2-(thiophen-2-yl)Et)sulfonyl)carbamoyl	38	4-Methiophen-2-yl	39	4,5-diMethiophen-2-yl
40	thiophen-3-ylMe	41	Ph	42	*p*-MePh
43	*m*-MePh	44	*o*-ClPh	45	*o*-BrPh
46	*o*-MePh	47	(Bzsulfonyl)carbamoyl	48	((4-MeBz)sulfonyl)carbamoyl
49	((3,5-diMeBz)sulfonyl)carbamoyl	50	((4-((1H-imidazol-2-yl)Me)Bz)sulfonyl)carbamoyl	51	(((4-Mecyclohexyl)Me)sulfonyl)carbamoyl
52	((4-EtBz)sulfonyl)carbamoyl	53	(Br-imino)(3-ClPh)Me	54	(Br-imino)(3-BrPh)Me
55	(Cl-imino)(3-Clph)Me	56	(Cl-imino)(2- ClPh)Me	57	imino(o-tolyl)Me
58	4-Cl-1H-pyrazol-1-yl	59	4,5-diCl-1H-pyrazol-1-yl	60	5-Cl-1H-pyrazol-1-yl
61	3-Cl-1H-pyrazol-1-yl	62	3-Br-1H-pyrazol-1-yl	63	4-Br-1H-pyrazol-1-yl
64	5-Br-1H-pyrazol-1-yl	65	4,5-diBr-1H-pyrazol-1-yl	66	3,4,5-triBr-1H-pyrazol-1-yl
67	5-iodo-1H-pyrazol-1-yl	68	4-iodo-1H-pyrazol-1-yl	69	3-iodo-1H-pyrazol-1-yl
70	3,4-diiodo-1H-pyrazol-1-yl	71	3,4,5-triiodo-1H-pyrazol-1-yl	72	3-amino-1H-pyrazol-1-yl
73	4-amino-1H-pyrazol-1-yl	74	5-amino-1H-pyrazol-1-yl	75	5-Me-1H-pyrazol-1-yl
76	((5-Et-1H-pyrazol-1-yl)sulfonyl)carbamoyl	77	4-Me-1H-pyrazol-1-yl	78	4,5-diMe-1H-pyrazol-1-yl
79	5-Et-4-Me-1H-pyrazol-1-yl	80	pyridazin-3-yl	81	pyridazin-4-yl)
82	pyrimidin-4-yl	83	1,3,5-triazin-2-yl	84	pyrimidin-2-yl
85	pyrazin-2-yl	86	cyclohexyl	87	piperidin-1-yl
88	tetrahydropyridazin-1(2H)-yl	89	piperazin-1-yl	90	1,2,4-triazinan-1-yl
91	(indolizin-2-ylsulfonyl)carbamoyl	92	((5-Ph-1H-pyrrol-3-yl)sulfonyl)carbamoyl	93	((5-Phthiophen-3-yl)sulfonyl)carbamoyl
94	([1,1'-biPh]-4-ylsulfonyl)carbamoyl	95	((6-Phpyridin-3-yl)sulfonyl)carbamoyl	96	((4-(pyridin-2-yl)Ph)sulfonyl)carbamoyl
97	((4-(1H-pyrazol-1-yl)Ph)sulfonyl)carbamoyl	98	((4-(thiazol-2-yl)Ph)sulfonyl)carbamoyl	99	((4-(thiophen-2-yl)Ph)sulfonyl)carbamoyl
100	((4-(1H-pyrrol-2-yl)Ph)sulfonyl)carbamoyl	101	((4-(pyrimidin-2-yl)Ph)sulfonyl)carbamoyl	102	((3',5'-diMe-[1,1'-biPh]-4-yl)sulfonyl)carbamoyl
103	((3',4'-diMe-[1,1'-biPh]-4-yl)sulfonyl)carbamoyl	104	((3',4',5'-diMe-[1,1'-biPh]-4-yl)sulfonyl)carbamoyl	105	((4-cyclohexylPh)sulfonyl)carbamoyl
106	((6,6-diMeheptyl)sulfonyl)carbamoyl	107	((6-Meheptyl)sulfonyl)carbamoyl	108	((3,3-diMebutyl)sulfonyl)carbamoyl

109	(S)-((6-Meoctyl)sulfonyl)carbamoyl	110	((4-cyclopropylbutyl)sulfonyl)carbamoyl	111	((4-cyclobutylbutyl)sulfonyl)carbamoyl
112	((4-cyclopentylbutyl)sulfonyl)carbamoyl	113	((4-cyclohexylbutyl)sulfonyl)carbamoyl	114	((2-(1H-imidazol-2-yl)Et)sulfonyl)carbamoyl
115	(S)-((3-Br-2-(thiazol-2-yl)propyl)sulfonyl)carbamoyl	116	((4-(pyridin-3-yl)butyl)sulfonyl)carbamoyl	117	((2-(1,3,4-thiadiazol-2-yl)Et)sulfonyl)carbamoyl
118	(S)-((2-Br-2-(1,3,4-thiadiazol-2-yl)Et)sulfonyl)carbamoyl	119	((4-(1H-imidazol-2-yl)butyl)sulfonyl)carbamoyl	120	((3-(neopentylamino)propyl)sulfonyl)carbamoyl
121	((5-(Me-amino)pentyl)sulfonyl)carbamoyl	122	(S)-((2-mercapto-3,3-diMebutyl)sulfonyl)carbamoyl	123	(R)-((6-aminooctyl)sulfonyl)carbamoyl
124	(3R,4S)-((3-Et-4-phosphinopentyl)sulfonyl)carbamoyl	125	((cycloprop-2-en-1-ylMe)sulfonyl)carbamoyl	126	((4-(5-F-1H-pyrazol-1-yl)Ph)sulfonyl)carbamoyl
127	((4-(4-F-1H-pyrazol-1-yl)Ph)sulfonyl)carbamoyl	128	((4-(3-F-1H-pyrazol-1-yl)Ph)sulfonyl)carbamoyl	129	((4-(3,4-diF-1H-pyrazol-1-yl)Ph)sulfonyl)carbamoyl
130	((4-(3,4,5-triF-1H-pyrazol-1-yl)Ph)sulfonyl)carbamoyl	131	((4-(4,5-diF-1H-pyrazol-1-yl)Ph)sulfonyl)carbamoyl	132	((4-(3,5-diF-1H-pyrazol-1-yl)Ph)sulfonyl)carbamoyl
133	((4-(3-Br-1H-pyrazol-1-yl)Ph)sulfonyl)carbamoyl	134	((4-(4-Br-1H-pyrazol-1-yl)Ph)sulfonyl)carbamoyl	135	((4-(5-Br-1H-pyrazol-1-yl)Ph)sulfonyl)carbamoyl
136	((4-(4,5-diBr-1H-pyrazol-1-yl)Ph)sulfonyl)carbamoyl	137	((4-(3,4-diBr-1H-pyrazol-1-yl)Ph)sulfonyl)carbamoyl	138	((4-(3,5-diBr-1H-pyrazol-1-yl)Ph)sulfonyl)carbamoyl
139	((4-(3,4,5-triBr-1H-pyrazol-1-yl)Ph)sulfonyl)carbamoyl	140	((4-(5-mercapto-1H-pyrazol-1-yl)Ph)sulfonyl)carbamoyl	141	((4-(4-mercapto-1H-pyrazol-1-yl)Ph)sulfonyl)carbamoyl
142	((4-(3-mercapto-1H-pyrazol-1-yl)Ph)sulfonyl)carbamoyl	143	((4-(3,4-dimercapto-1H-pyrazol-1-yl)Ph)sulfonyl)carbamoyl	144	((4-(4,5-dimercapto-1H-pyrazol-1-yl)Ph)sulfonyl)carbamoyl
145	((4-(3,5-dimercapto-1H-pyrazol-1-yl)Ph)sulfonyl)carbamoyl	146	((4-(3,4,5-trimercapto-1H-pyrazol-1-yl)Ph)sulfonyl)carbamoyl	147	((4-(3-iodo-1H-pyrazol-1-yl)Ph)sulfonyl)carbamoyl
148	((4-(4-iodo-1H-pyrazol-1-yl)Ph)sulfonyl)carbamoyl	149	((4-(5-iodo-1H-pyrazol-1-yl)Ph)sulfonyl)carbamoyl	150	((4-(4,5-diiodo-1H-pyrazol-1-yl)Ph)sulfonyl)carbamoyl
151	((4-(3,4-diiodo-1H-pyrazol-1-yl)Ph)sulfonyl)carbamoyl	152	((4-(3,4,5-triiodo-1H-pyrazol-1-yl)Ph)sulfonyl)carbamoyl	153	((4-(3,5-diiodo-1H-pyrazol-1-yl)Ph)sulfonyl)carbamoyl
154	((4-(3-Cl-1H-pyrazol-1-yl)Ph)sulfonyl)carbamoyl	155	((4-(4-Cl-1H-pyrazol-1-yl)Ph)sulfonyl)carbamoyl	156	((4-(5-Cl-1H-pyrazol-1-yl)Ph)sulfonyl)carbamoyl
157	((4-(4,5-diCl-1H-pyrazol-1-yl)Ph)sulfonyl)carbamoyl	158	((4-(3,5-diCl-1H-pyrazol-1-yl)Ph)sulfonyl)carbamoyl	159	((4-(3,4-diCl-1H-pyrazol-1-yl)Ph)sulfonyl)carbamoyl
160	((4-(3,4,5-triCl-1H-pyrazol-1-yl)Ph)sulfonyl)carbamoyl	161	((4-(3-amino-1H-pyrazol-1-yl)Ph)sulfonyl)carbamoyl	162	((4-(4-amino-1H-pyrazol-1-yl)Ph)sulfonyl)carbamoyl
163	((4-(5-amino-1H-pyrazol-1-yl)Ph)sulfonyl)carbamoyl	164	((4-(4,5-diamino-1H-pyrazol-1-yl)Ph)sulfonyl)carbamoyl	165	((4-(3,5-diamino-1H-pyrazol-1-yl)Ph)sulfonyl)carbamoyl
166	((4-(3,4-diamino-1H-pyrazol-1-yl)Ph)sulfonyl)carbamoyl	167	((4-(3,4,5-triamino-1H-pyrazol-1-yl)Ph)sulfonyl)carbamoyl	168	((4-(3-Me-1H-pyrazol-1-yl)Ph)sulfonyl)carbamoyl
169	((4-(4-Me-1H-pyrazol-1-yl)Ph)sulfonyl)carbamoyl	170	((4-(5-Me-1H-pyrazol-1-yl)Ph)sulfonyl)carbamoyl	171	((4-(4,5-diMe-1H-pyrazol-1-yl)Ph)sulfonyl)carbamoyl
172	((4-(3,5-diMe-1H-pyrazol-1-yl)Ph)sulfonyl)carbamoyl	173	((4-(3,4-diMe-1H-pyrazol-1-yl)Ph)sulfonyl)carbamoyl	174	((4-(3,4,5-triMe-1H-pyrazol-1-yl)Ph)sulfonyl)carbamoyl
175	((4-(5-Et-1H-pyrazol-1-yl)Ph)sulfonyl)carbamoyl	176	((4-(4-Et-1H-pyrazol-1-yl)Ph)sulfonyl)carbamoyl	177	((4-(5-Et-4-Me-1H-pyrazol-1-yl)Ph)sulfonyl)carbamoyl
178	((4-(5-Et-3,4-diMe-1H-pyrazol-1-yl)Ph)sulfonyl)carbamoyl	179	((4-(5-(Methio)-1H-pyrazol-1-yl)Ph)sulfonyl)carbamoyl	180	((4-(4-mercapto-5-(Methio)-1H-pyrazol-1-yl)Ph)sulfonyl)carbamoyl
181	((4-(4,5-bis(Methio)-1H-pyrazol-1-yl)Ph)sulfonyl)carbamoyl	182	((4-(3-Me-4,5-bis(Methio)-1H-pyrazol-1-yl)Ph)sulfonyl)carbamoyl	183	((4-(5-(aminothio)-1H-pyrazol-1-yl)phenyl)sulfonyl)carbamoyl
184	((4-(4-(aminothio)-1H-pyrazol-1-yl)Ph)sulfonyl)carbamoyl	185	((4-(4-(aminothio)-5-mercapto-1H-pyrazol-1-yl)Ph)sulfonyl)carbamoyl	186	((4-(4,5-bis(aminothio)-1H-pyrazol-1-yl)Ph)sulfonyl)carbamoyl
187	((4-(5H-tetrazol-5-yl)Ph)sulfonyl)carbamoyl	188	((4-(1H-imidazol-1-yl)Ph)sulfonyl)carbamoyl	189	((4-(1H-1,2,4-triazol-1-yl)Ph)sulfonyl)carbamoyl
190	((4-(1H-tetrazol-1-yl)Ph)sulfonyl)carbamoyl	191	(R)-((2-Ph-2H-pyrrol-4-y)sulfonyl)carbamoyl l	192	((4-(pyrazin-2-yl)Ph)sulfonyl)carbamoyl
193	((4-(pyridazin-3-yl)Ph)sulfonyl)carbamoyl	194	((4-(piperazin-1-yl)Ph)sulfonyl)carbamoyl	195	((3H-indol-2-yl)sulfonyl)carbamoyl
196	((7H-purin-8-yl))sulfonyl)carbamoyl	197	(S)-((1,8a-dihydroindolizin-2-yl)sulfonyl)carbamoyl	198	((isoquinolin-6-yl)sulfonyl)carbamoyl
199	((quinolin-6-yl)sulfonyl)carbamoyl	200	((naphthalen-2-y)sulfonyl)carbamoyl l	201	((quinolin-8-y)sulfonyl)carbamoyl l
202	((isoquinolin-8-yl)sulfonyl)carbamoyl	203	((isoquinolin-5-yl)sulfonyl)carbamoyl	204	((quinolin-5-yl))sulfonyl)carbamoyl
205	((thianthren-2-yl)sulfonyl)carbamoyl	206	((thianthren-1-yl)sulfonyl)carbamoyl	207	((acridin-9-yl)sulfonyl)carbamoyl
208	((acridin-4-yl)sulfonyl)carbamoyl	209	((acridin-3-yl)sulfonyl)carbamoyl	210	((anthracen-9-yl)sulfonyl)carbamoyl
211	((anthracen-1-yl)sulfonyl)carbamoyl	212	((anthracen-2-yl)sulfonyl)carbamoyl	213	((9H-carbazol-9-yl)sulfonyl)carbamoyl
214	((9H-carbazol-1-yl)sulfonyl)carbamoyl	215	((9H-carbazol-2-yl)sulfonyl)carbamoyl	216	((5-Me-9H-carbazol-2-yl)sulfonyl)carbamoyl
217	(((R)-5-(Meamino)hexyl)sulfonyl)carbamoyl	218	(R)-((5-(Etamino)hexyl)sulfonyl)carbamoyl	219	(R)-((5-(isopropylamino)hexyl)sulfonyl)carbamoyl
220	(3R,5R)-((5-(Etamino)-3-Mehexyl)sulfonyl)carbamoyl	221	((aminoMe)sulfonyl)carbamoyl		

* R_1-groups : fragments 1-7, 11, **18;** R_2 and R_3 groups : fragments 4 ; 8 - 20. R_4 -groups: fragments 2, 4, 8-90 ; R_5-groups: fragments 1-221.

3.5.2. *In Silico* Screening of Library of EHBs

The focused library of 125,915 analogs was further screened for molecular structures matching the 3D-QSAR PH4 pharmacophore model Hypo1 of RdRp inhibition. 329 EHBs mapped to at least 4 features of the pharmacophore. These best fitting analogs (PH4 hits) then underwent complexation QSAR model screening. The computed GFE of RdRp-EHBx complex formation, their components, and predicted half-maximal inhibitory concentrations IC_{50}^{pre} calculated from the correlation Equation B (Table 3) are listed in Table 7.

Table 7. GFE and their components for the top scoring 304 virtual EHB analogs. The analog numbering concatenates the index of each substituent R_1 to R_5 with the substituent numbers taken from Table 6.

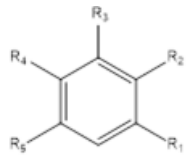

N°	Designed Analogs	M_W [a] (g/mol)	$\Delta\Delta H_{MM}$ [b] (kcal/mol)	$\Delta\Delta G_{sol}$ [c] (kcal/mol)	$\Delta\Delta TS_{vib}$ [d] (kcal/mol)	$\Delta\Delta G_{com}$ [e] (kcal/mol)	IC_{50}^{pre} [f] (nM)
Ref	EHB1	492	0	0	0	0	23[g]
1	2-11-17-21-114	486	8.40	-2.19	0.77	5.44	407
2	2-9-17-85-27	494	1.99	-0.74	1.54	-0.29	28
3	2-18-17-26-47	493	3.37	-2.12	2.39	-1.13	19
4	2-17-17-2-200	475	8.91	1.57	-0.10	10.58	4530
5	2-17-11-29-114	468	11.72	-2.17	1.59	7.96	1329
6	2-17-17-80-22	468	3.34	-0.21	0.47	2.66	110
7	2-17-9-26-114	496	7.36	-2.34	3.01	2.02	82
8	2-10-10-83-221	497	8.67	-3.88	-4.62	9.42	2628
9	2-9-9-34-221	473	9.02	-3.59	1.65	3.78	187
10	2-9-17-2-200	489	5.45	-3.00	-0.40	2.85	121
11	2-9-17-81-125	464	-12.78	-1.57	-7.84	-6.51	1.5
12	2-17-17-11-101	490	8.20	-4.28	-4.21	8.14	1445
13	2-15-17-2-117	489	10.15	-4.00	-0.94	7.09	883
14	2-17-17-11-93	494	6.81	1.43	-3.35	11.6	7319
15	2-9-8-9-114	472	8.08	-3.54	1.26	3.29	149
16	2-20-9-17-21	469	9.98	-4.99	0.50	4.49	261
17	2-17-8-11-119	488	6.42	-1.95	2.22	2.25	91
18	2-17-9-10-114	462	10.12	-2.49	0.54	7.09	881
19	2-9-9-13-114	488	7.34	-2.18	0.38	4.78	437
20	2-17-17-20-22	469	8.75	-2.81	-0.68	6.63	710
21	2-8-8-17-114	474	4.70	-2.55	1.40	0.75	45
22	2-19-11-4-21	453	13.52	-2.65	4.86	6.01	532
23	2-9-19-8-24	491	6.78	2.50	9.01	0.27	36
24	2-8-9-4-114	490	7.52	-1.60	1.89	4.02	210
25	2-12-11-15-22	500	7.41	-4.88	2.50	0.04	32
26	2-17-10-11-119	493	4.51	1.99	-2.40	8.90	2067
27	2-17-9-4-37	476	12.44	-3.10	2.06	7.28	966
28	2-9-8-8-114	488	5.56	-4.01	0.77	0.78	46
29	2-11-13-17-117	494	2.79	-0.58	-2.69	4.89	315
30	2-17-17-18-168	491	7.86	-3.48	-3.65	8.03	1372
31	2-11-17-8-114	460	5.81	-2.59	0.76	2.46	101
32	2-19-4-17-114	475	7.88	-1.82	2.90	3.16	140
33	2-17-19-9-119	485	8.18	0.06	3.55	4.69	287
34	2-17-17-18-188	477	0.07	-0.35	-3.66	3.39	156
35	2-8-11-9-114	474	4.45	-1.88	-0.61	3.17	141
36	2-17-19-17-121	448	8.84	-2.70	5.41	0.73	45
37	2-18-17-12-195	499	6.71	-1.49	-1.89	7.11	892
38	2-18-9-10-28	480	7.63	-5.08	2.90	-0.35	27
39	2-13-17-8-114	490	6.83	-2.99	-1.17	5.01	333

N°	Designed Analogs	M_W [a] (g/mol)	$\Delta\Delta H_{MM}$ [b] (kcal/mol)	$\Delta\Delta G_{sol}$ [c] (kcal/mol)	$\Delta\Delta TS_{vib}$ [d] (kcal/mol)	$\Delta\Delta G_{com}$ [e] (kcal/mol)	IC_{50}^{pre} [f] (nM)
40	5-19-17-2-114	489	8.21	-3.84	-1.31	5.68	456
41	5-18-10-9-26	468	9.12	-2.50	3.34	3.27	147
42	5-17-17-18-97	494	8.97	-4.54	-2.49	6.92	817
43	5-17-17-21-114	487	5.14	0.99	2.18	3.95	203
44	5-11-13-18-27	496	3.91	-4.37	-0.13	-0.33	27
45	5-11-17-10-114	481	4.51	1.24	-4.47	10.22	3837
46	5-9-13-17-114	491	3.12	1.18	0.13	4.17	224
47	5-17-17-8-201	494	4.99	-0.95	-1.46	5.51	420
48	5-17-17-8-114	461	3.25	0.88	1.21	2.92	125
49	7-19-11-4-26	479	5.46	-2.06	3.17	0.23	35
50	7-17-17-2-199	490	4.79	-2.26	-2.06	4.60	275
51	7-17-17-2-201	490	1.27	-0.05	-2.01	3.23	144
52	7-17-17-2-47	453	1.95	2.33	-0.83	5.11	349
53	7-9-17-17-24	446	2.98	1.77	4.61	0.14	34
54	7-17-9-2-117	489	5.14	-1.59	0.35	3.20	142
55	7-8-17-2-47	483	-2.08	-1.61	-1.28	-2.41	10
56	7-17-13-19-22	479	9.23	0.67	2.09	7.81	1240
57	7-10-17-4-114	495	7.73	-1.91	-3.97	9.79	3131
58	7-11-9-17-195	479	-0.83	3.32	-2.96	5.45	409
59	7-15-17-8-114	486	1.69	-0.78	-0.96	1.86	76
60	7-18-8-17-195	494	-1.51	0.74	-0.07	-0.70	23
61	7-17-8-18-197	496	1.17	-1.92	1.72	-2.47	10
62	7-8-19-17-114	487	-1.24	0.57	0.53	-1.21	18
63	7-17-12-17-114	476	4.55	-0.93	-2.60	6.22	588
64	7-9-9-15-114	484	1.63	-0.68	3.45	-2.51	10
65	7-17-15-18-37	487	6.26	-0.92	2.92	2.42	99
66	7-17-17-11-92	491	-3.55	5.64	-4.15	6.23	591
67	1-15-17-2-195	493	2.11	-0.39	-1.72	3.44	160
68	1-18-11-83-25	485	3.12	-0.37	-0.30	3.05	133
69	1-17-9-17-98	494	5.20	-3.22	-2.93	4.91	318
70	1-4-17-2-114	476	7.79	-1.13	2.57	4.09	216
71	1-17-17-81-114	493	5.71	-0.62	-3.37	8.46	1675
72	1-4-17-75-221	462	9.57	-0.21	-1.62	10.97	5451
73	1-17-9-2-195	479	3.31	0.49	-0.29	4.08	216
74	1-8-17-29-121	488	5.69	1.03	1.17	5.54	428
75	1-11-9-34-125	499	1.39	0.03	-7.03	8.45	1671
76	1-17-19-17-100	491	2.92	-2.14	-1.66	2.44	100
77	1-15-17-2-25	432	6.13	-2.22	4.75	-0.84	21
78	1-11-17-18-97	494	-0.13	-3.30	-2.02	-1.40	16
79	1-19-17-25-114	485	4.32	0.16	0.40	4.07	214
80	1-17-17-21-114	471	6.28	0.39	-0.75	7.41	1028
81	1-11-11-15-37	491	3.10	0.44	0.46	3.08	135
82	1-10-10-19-26	487	9.04	-2.49	-1.48	8.04	1378
83	1-18-9-10-117	497	2.85	0.43	-6.70	9.98	3425
84	1-15-15-9-114	485	8.42	-0.43	3.48	4.50	262
85	1-17-17-10-21	411	8.16	-2.76	-0.86	6.26	598
86	1-17-11-8-114	461	3.73	-0.45	1.43	1.85	76
87	1-4-15-17-21	437	7.24	-2.03	4.96	0.24	36
88	1-19-19-8-21	465	-1.10	-0.10	3.09	-4.30	4.2
89	1-18-9-8-117	492	5.20	0.39	0.47	5.12	350
90	1-19-10-18-110	495	-1.11	-0.90	-0.69	-1.32	17
91	1-9-10-10-114	498	5.26	-1.32	-2.98	6.93	819
92	1-18-8-9-114	474	3.99	1.22	-0.83	6.03	538
93	1-17-10-18-47	460	4.65	-2.58	-3.97	6.05	542
94	1-11-11-8-51	493	-2.80	4.85	1.05	1.00	51
95	1-9-17-8-116	498	0.52	-0.49	-0.03	0.05	33
96	1-17-17-13-199	494	7.28	-0.65	-3.14	9.76	3092
97	1-15-17-9-114	457	7.18	-3.00	0.10	4.08	216
98	1-8-9-17-199	492	3.60	-1.60	-3.27	5.26	375
99	1-17-17-8-121	450	3.71	-0.05	2.85	0.81	47
100	1-15-17-15-117	489	9.02	-2.71	-0.77	7.08	878

N°	Designed Analogs	M_W [a] (g/mol)	$\Delta\Delta H_{MM}$ [b] (kcal/mol)	$\Delta\Delta G_{sol}$ [c] (kcal/mol)	$\Delta\Delta TS_{vib}$ [d] (kcal/mol)	$\Delta\Delta G_{com}$ [e] (kcal/mol)	IC_{50}^{pre} [f] (nM)
101	1-18-9-17-52	468	4.12	3.81	1.58	6.35	623
102	1-9-4-18-121	481	3.63	-0.76	4.80	-1.93	13
103	1-17-17-15-119	471	5.29	1.61	1.36	5.53	425
104	1-15-17-4-117	493	12.01	-3.48	-1.81	10.35	4076
105	1-9-18-9-119	486	1.40	2.44	2.26	1.58	67
106	1-17-17-8-117	463	7.09	-1.55	-2.73	8.27	1537
107	1-10-18-15-114	493	5.49	-0.06	-0.62	6.05	542
108	1-11-9-11-199	494	4.87	-1.12	-2.77	6.53	678
109	1-4-11-18-27	466	2.24	-1.59	2.48	-1.83	13
110	1-17-17-9-124	465	4.96	4.22	2.37	6.81	774
111	3-18-10-17-47	473	2.24	4.43	-5.49	12.16	9516
112	3-17-10-8-114	492	4.31	-0.58	-3.28	7.01	851
113	3-11-15-17-21	434	5.20	-2.12	1.42	1.66	69
114	3-11-19-17-117	491	3.74	1.12	-1.16	6.02	536
115	3-9-9-10-114	490	6.32	-0.63	-1.03	6.72	744
116	3-11-11-17-201	493	-1.33	6.84	-4.76	10.27	3921
117	3-9-15-18-47	481	13.05	-1.87	-0.38	11.55	7152
118	4-13-17-18-110	480	6.37	-2.61	0.43	3.32	151
119	4-9-8-18-37	492	7.49	-1.59	0.14	5.76	474
120	4-8-12-19-26	499	6.96	-0.36	0.71	5.90	504
121	4-17-11-17-163	496	9.72	-2.60	-3.99	11.11	5828
122	4-11-11-11-28	467	14.39	-3.32	1.51	9.56	2815
123	1-8-17-9-195	480	-0.04	-0.18	-0.59	0.38	38
124	1-8-17-9-37	475	4.15	-1.52	1.63	1.00	51
125	1-8-17-9-116	498	0.09	-0.56	-0.08	-0.38	27
126	2-8-17-9-114	458	7.07	-3.59	2.20	1.28	58
127	2-8-17-9-117	476	6.48	-2.83	1.04	2.61	108
128	3-8-17-9-37	488	3.99	-1.13	0.05	2.80	118
129	4-8-17-9-114	461	8.34	-1.39	1.14	5.81	485
130	7-8-17-9-26	446	3.42	-2.98	5.26	-4.81	3.3
131	7-8-17-9-114	472	1.63	-1.11	1.71	-1.19	18
132	1-17-8-2-195	495	2.51	-2.01	-0.61	1.11	54
133	1-11-15-29-114	497	10.02	1.68	-0.35	12.05	9030
134	1-18-17-82-26	482	8.15	-1.14	0.98	6.02	535
135	1-15-9-80-25	495	7.25	-2.06	0.36	4.83	307
136	1-13-15-21-221	480	5.79	-0.23	6.55	-0.99	20
137	1-17-10-34-221	481	5.70	-1.60	-4.79	8.88	2047
138	1-11-18-17-97	494	2.00	-1.68	-2.55	2.87	122
139	1-17-8-15-22	449	5.96	-1.16	4.18	0.62	43
140	1-17-18-9-97	492	2.46	-2.24	-2.16	2.37	97
141	1-9-18-17-97	492	1.84	-3.68	-1.78	-0.06	31
142	1-13-11-87-221	495	4.11	-0.35	1.99	1.76	73
143	1-15-9-9-119	499	1.08	2.34	4.66	-1.24	18
144	1-12-11-15-221	442	5.90	-2.19	1.46	2.25	91
145	1-10-9-11-114	479	6.84	-0.88	0.40	5.56	432
146	1-4-11-18-27	466	5.53	2.71	4.09	4.15	223
147	1-8-18-17-112	490	4.98	0.50	7.74	-0.27	28
148	1-18-13-11-108	482	2.86	4.49	3.12	4.23	231
149	1-9-17-11-108	435	4.33	3.31	6.32	1.31	59
150	1-18-10-11-48	490	0.82	4.05	-0.95	5.82	486

N°	Designed Analogs	M_W [a] (g/mol)	$\Delta\Delta H_{MM}$ [b] (kcal/mol)	$\Delta\Delta G_{sol}$ [c] (kcal/mol)	$\Delta\Delta TS_{vib}$ [d] (kcal/mol)	$\Delta\Delta G_{com}$ [e] (kcal/mol)	IC_{50}^{pre} [f] (nM)
151	1-17-17-20-27	482	5.53	2.51	-0.47	8.51	1722
152	1-12-18-12-21	489	6.39	-1.32	2.53	2.54	105
153	1-9-18-11-27	448	2.92	2.34	5.16	0.10	33
154	1-11-4-11-26	453	8.89	-2.57	1.16	5.15	356
155	1-20-18-17-22	485	4.84	4.06	0.89	8.00	1356
156	1-4-18-11-23	468	6.05	4.04	3.02	7.08	879
157	1-18-17-13-28	478	2.95	0.50	3.89	-0.44	26
158	1-17-12-4-76	496	9.94	-1.99	-1.45	9.39	2594
159	1-18-11-4-195	499	2.72	6.97	-1.38	11.07	5699
160	1-8-17-18-28	462	2.06	-2.04	6.01	-6.00	1.9
161	1-17-18-10-76	464	5.41	-0.44	-2.27	7.24	949
162	1-13-10-15-125	482	-4.19	-1.78	0.83	-6.80	1.3
163	1-17-11-9-124	481	3.90	1.12	3.57	1.46	63
164	1-11-4-18-51	494	-0.01	3.51	2.46	1.04	52
165	2-17-17-2-195	464	7.28	-0.82	0.66	5.80	482
166	2-13-17-77-221	475	10.05	1.25	4.29	7.02	854
167	2-8-17-25-21	460	4.24	-1.36	3.26	-0.38	27
168	2-17-17-27-221	431	10.74	1.41	6.17	5.98	526
169	2-17-11-17-98	495	6.02	-0.77	-2.79	8.04	1377
170	2-17-9-84-108	496	2.23	-3.40	2.02	-3.19	7.1
171	2-17-9-82-25	466	9.43	-3.21	0.69	5.52	423
172	2-17-17-29-48	462	9.44	-3.02	-2.05	8.47	1684
173	2-9-18-17-97	491	3.76	-4.69	-0.78	-0.16	29
174	2-17-4-86-221	449	11.84	-4.80	4.84	2.19	89
175	2-4-9-29-21	460	12.54	-2.28	4.01	6.24	593
176	2-19-4-29-26	487	13.03	-2.83	2.17	8.03	1373
177	2-8-15-29-21	472	10.31	-3.39	2.16	4.76	297
178	2-11-19-29-27	485	8.60	-2.07	2.26	4.28	236
179	2-11-8-17-114	460	5.51	-3.00	2.02	0.49	40
180	2-13-9-11-114	490	8.82	-2.80	-1.04	7.06	872
181	2-8-10-18-108	484	2.45	-7.30	3.70	-8.55	0.58
182	2-8-9-8-121	493	-2.49	-1.62	4.19	-8.30	0.65
183	2-18-17-10-108	454	7.54	-4.39	4.48	-1.34	17
184	2-4-17-13-21	454	11.52	-4.35	2.22	4.95	324
185	2-4-9-4-114	492	12.63	-2.77	0.37	9.50	2728
186	2-9-12-9-25	451	8.40	-5.56	3.26	-0.42	26
187	2-4-9-18-48	485	4.81	0.28	-1.32	6.42	644
188	2-11-9-4-114	476	9.69	-2.91	1.71	5.07	343
189	2-17-17-9-25	388	12.00	-3.89	0.85	7.26	957
190	2-18-4-17-25	421	9.71	-0.95	1.19	7.56	1102
191	2-18-4-4-24	497	10.13	-0.22	2.98	6.94	824
192	2-15-15-18-27	473	10.71	-2.63	6.78	1.30	59
193	2-17-11-9-26	418	8.47	-3.79	5.53	-0.86	21
194	2-8-11-8-114	490	2.49	-1.88	-0.88	1.49	64
195	2-17-17-19-119	471	12.16	-0.58	0.71	10.86	5184
196	2-9-17-15-195	477	4.31	-3.11	0.02	1.18	55
197	2-10-18-9-48	488	2.66	-1.34	-0.14	1.47	63
198	2-9-15-9-119	498	-0.17	0.72	5.85	-5.29	2.7
199	2-13-18-10-27	498	5.58	-4.07	2.05	-0.54	25
200	2-9-4-17-37	476	7.32	0.38	1.99	5.71	463

N°	Designed Analogs	M_W [a] (g/mol)	$\Delta\Delta H_{MM}$ [b] (kcal/mol)	$\Delta\Delta G_{sol}$ [c] (kcal/mol)	$\Delta\Delta TS_{vib}$ [d] (kcal/mol)	$\Delta\Delta G_{com}$ [e] (kcal/mol)	IC_{50}^{pre} [f] (nM)
201	2-10-18-17-195	484	5.27	-1.25	-3.27	7.29	971
202	2-8-10-18-27	482	2.05	-4.01	3.29	-5.25	2.7
203	2-4-12-17-76	495	5.29	-1.17	-0.12	4.24	232
204	2-17-18-15-125	415	10.03	-1.80	-1.56	9.78	3123
205	2-10-11-17-28	467	4.26	0.61	3.07	1.80	74
206	2-11-11-9-28	462	3.00	1.19	2.88	1.31	59
207	2-9-4-9-221	409	10.10	-6.03	1.54	2.52	104
208	2-12-12-11-125	485	5.08	-2.50	-6.71	9.30	2488
209	2-4-4-11-27	482	8.42	-0.48	4.25	3.69	180
210	3-8-13-17-221	439	3.97	-4.63	-0.61	-0.06	31
211	3-17-9-11-116	497	1.19	6.45	-0.77	8.41	1641
212	3-17-9-83-221	456	7.69	-2.16	-2.08	7.60	1123
213	3-9-8-17-114	472	-4.25	6.21	-0.32	2.28	93
214	3-17-17-11-195	465	5.16	-0.42	-6.18	10.92	5316
215	3-18-8-17-122	495	1.92	3.94	2.55	3.31	150
216	3-10-11-17-47	474	1.00	4.18	-5.90	11.07	5715
217	3-9-10-18-108	482	0.68	2.41	2.38	0.71	44
218	3-17-11-9-195	479	1.51	0.72	-2.69	4.92	319
219	3-17-18-17-97	491	2.82	-1.18	-3.67	5.31	383
220	3-10-15-11-125	464	11.3	-0.88	1.42	8.99	2154
221	3-9-15-2-76	499	-3.55	4.04	-0.12	0.61	42
222	3-18-4-17-76	475	1.28	5.83	-2.04	9.14	2311
223	3-9-18-17-76	457	0.45	5.08	1.33	4.20	228
224	3-17-17-10-91	483	5.15	-1.15	-8.10	12.10	9240
225	3-19-12-17-27	494	2.08	-1.35	0.06	0.67	43
226	3-4-9-11-125	448	12.93	-4.08	-5.41	14.26	25515
227	3-17-11-10-121	484	2.35	0.64	-0.14	3.13	138
228	4-4-10-11-125	458	8.82	-4.39	-6.22	10.64	4671
229	4-18-10-18-27	470	10.75	-3.18	1.32	6.25	595
230	5-4-9-77-221	492	14.69	-3.30	4.08	7.32	983
231	5-17-11-2-195	497	2.90	0.36	-1.33	4.59	274
232	5-11-17-15-25	435	7.39	-3.00	1.99	2.40	98
233	5-18-17-17-100	493	3.77	-3.07	-3.54	4.23	231
234	5-4-9-89-221	496	7.16	-1.12	4.85	1.19	56
235	5-17-11-17-97	495	5.97	-6.25	-3.45	3.17	141
236	5-17-17-18-100	493	3.77	-1.90	-1.38	3.25	146
237	5-17-15-80-25	497	10.21	-3.36	-0.28	7.13	900
238	5-17-9-2-121	479	9.96	-2.19	2.63	5.14	354
239	5-9-11-2-76	490	3.56	-4.15	1.67	-2.27	11
240	5-17-11-8-23	467	4.72	-3.47	3.14	-1.89	13
241	5-9-15-2-2	437	10.34	-3.10	4.87	2.37	97
242	5-9-19-2-27	491	5.32	-1.72	4.21	-0.61	24
243	5-4-4-29-25	493	14.42	-3.20	-0.65	11.88	8341
244	5-11-17-19-24	480	15.33	-0.50	2.92	11.92	8497
245	5-17-17-11-108	437	8.71	-0.72	3.91	4.09	216
246	5-9-19-11-221	425	8.31	-3.18	2.11	3.02	131
247	5-17-8-17-114	461	7.72	-6.14	2.04	-0.46	26
248	5-10-17-17-114	465	8.22	-1.33	-2.80	9.70	2998
249	5-11-9-8-27	479	2.41	-2.94	1.66	-2.19	11
250	5-17-18-17-119	474	4.29	2.76	1.47	5.58	435

N°	Designed Analogs	M_W [a] (g/mol)	$\Delta\Delta H_{MM}$ [b] (kcal/mol)	$\Delta\Delta G_{sol}$ [c] (kcal/mol)	$\Delta\Delta TS_{vib}$ [d] (kcal/mol)	$\Delta\Delta G_{com}$ [e] (kcal/mol)	IC_{50}^{pre} [f] (nM)
251	5-15-8-4-221	456	13.34	-4.75	1.97	6.62	710
252	5-8-11-8-221	442	4.26	-3.17	0.02	1.07	53
253	5-17-11-11-37	479	7.94	2.02	-0.14	10.11	3637
254	5-19-19-9-22	479	5.63	-4.65	5.09	-4.12	4.6
255	5-9-17-10-121	485	7.87	-4.37	0.88	2.62	109
256	5-11-17-11-114	463	7.12	-1.03	-0.60	6.69	734
257	5-18-17-17-123	479	0.75	4.53	3.12	2.15	87
258	5-17-9-15-121	478	5.03	-2.31	6.35	-3.63	5.8
259	5-4-9-11-114	493	9.05	-0.61	0.44	8.00	1354
260	5-11-17-11-123	496	-2.79	2.17	2.30	-2.93	8
261	5-18-4-18-24	497	7.32	-2.27	3.94	1.11	53
262	5-19-20-9-221	488	8.61	-3.48	-1.82	6.95	826
263	5-18-18-4-22	469	13.27	-3.08	5.63	4.56	270
264	5-17-4-11-22	455	9.87	0.43	3.03	7.27	963
265	5-17-17-18-190	496	8.35	-3.25	-4.37	9.46	2681
266	7-12-17-77-221	491	5.05	-5.34	0.13	-0.42	26
267	7-17-13-81-221	487	8.76	-1.86	0.88	6.02	535
268	7-17-17-2-116	496	2.03	-1.16	0.49	0.37	38
269	7-9-17-2-195	492	-0.50	3.53	-1.97	5.01	333
270	7-9-4-8-25	464	0.65	2.16	0.89	1.92	78
271	7-17-15-41-221	467	3.77	-1.08	2.58	0.12	34
272	7-10-17-2-47	487	0.50	-0.56	-1.9	1.84	75
273	7-17-15-77-221	471	7.62	-2.00	3.64	1.97	80
274	7-15-11-11-24	492	4.90	-0.78	2.6	1.52	65
275	7-9-12-2-21	482	2.32	-4.32	2.47	-4.47	3.9
276	7-9-9-2-76	485	0.13	-3.39	3.37	-6.62	1.4
277	7-17-17-8-21	420	3.13	-2.29	0.96	-0.11	30
278	7-17-4-4-23	482	5.40	-3.02	0.45	1.93	78
279	7-18-4-4-26	481	4.26	2.84	-0.92	8.02	1367
280	7-4-4-18-27	495	5.90	-1.30	0.66	3.94	202
281	7-18-17-4-21	437	8.44	2.80	0.92	10.32	4023
282	7-4-9-18-110	491	0.85	-0.86	0.78	-0.79	22
283	7-17-18-9-116	496	0.45	1.02	-0.68	2.16	87
284	7-17-13-13-221	455	8.72	-2.91	-3.66	9.47	2700
285	7-11-17-10-195	499	-1.13	5.20	-7.48	11.55	7153
286	7-9-9-17-198	489	-2.20	4.50	-1.47	3.77	187
287	7-8-17-4-47	486	1.63	-1.26	-1.10	1.47	63
288	7-11-17-9-119	486	-3.44	3.30	0.01	-0.15	30
289	7-17-14-10-221	490	9.77	-3.34	-4.18	10.61	4605
290	7-10-17-22-221	468	2.86	-2.57	1.19	-0.90	21
291	7-18-4-17-195	496	2.16	0.55	-5.32	8.03	1374
292	7-4-11-17-195	497	4.44	0.38	-7.06	11.88	8335
293	7-18-4-17-48	485	-1.82	5.95	-1.64	5.77	475
294	7-10-11-9-76	492	-1.84	-0.44	-3.16	0.88	48
295	7-17-18-17-97	491	1.85	-2.40	-3.51	2.96	127
296	7-17-17-29-111	482	6.41	-1.32	1.82	3.27	148
297	7-15-8-12-125	493	6.50	-1.31	-4.28	9.48	2705
298	7-17-17-12-125	434	9.84	-2.72	-1.17	8.30	1555
299	7-17-17-18-189	492	2.52	-3.95	-4.71	3.28	148
300	7-15-10-29-221	463	13.15	-4.88	-0.54	8.81	1978

N°	Designed Analogs	M_W [a] (g/mol)	$\Delta\Delta H_{MM}$ [b] (kcal/mol)	$\Delta\Delta G_{sol}$ [c] (kcal/mol)	$\Delta\Delta TS_{vib}$ [d] (kcal/mol)	$\Delta\Delta G_{com}$ [e] (kcal/mol)	IC_{50}^{pre} [f] (nM)
301	2-8-9-8-217	507	0.42	0.37	5.04	-4.26	4.3
302	2-8-9-8-218	521	-2.45	-1.09	7.23	-10.76	0.21
303	2-8-9-8-219	535	0.54	-2.66	7.75	-9.87	0.31
304	2-8-9-8-220	535	3.12	-3.22	7.99	-8.09	0.72

[a] Mw is molar mass of inhibitor. [b] $\Delta\Delta H_{MM}$ is the relative enthalpic contribution to the GFE change of the NS5RdRp-EHB complex formation $\Delta\Delta G_{com}$ (for details see footnote of Table 2); [c] $\Delta\Delta G_{sol}$ is the relative solvation GFE contribution to $\Delta\Delta G_{com}$; [d] $\Delta\Delta TS_{vib}$ is the relative (vibrational) entropic contribution to $\Delta\Delta G_{com}$; [e] $\Delta\Delta G_{com}$ is the relative Gibbs free energy (GFE) change related to the enzyme–inhibitor NS5RdRp-EHB complex formation $\Delta\Delta G_{com} = \Delta\Delta H_{MM} + \Delta\Delta G_{sol} - \Delta\Delta TS_{vib}$; [f] IC_{50}^{pre} is the predicted inhibition potency towards NS5RdRp; [g] Experimental value IC_{50}^{exp} is given for the reference inhibitor EHB1 instead of the predicted value.

3.6 Novel EHB Analogs

The design of virtual library of novel analogs was guided by structural information retrieved from the EHBx active conformation and was used for the selection of appropriate substituents (R_1- to R_5-groups). In order to identify which substituents lead to new inhibitor candidates with the highest predicted potencies towards the RdRp of Denv, we have prepared histograms of the frequency of occurrence of R_1- to R_5-groups among the 329 best fit PH4 hits (Figure 6). The histograms show that the R_1-groups 2, 1 and 7 were represented with the highest frequencies of occurrence (93), (86) and (59) among the 329 EHB hits. The R_2-groups and R_3-groups most frequently represented in this subset are 17 (99) and (110); 9 (45) and (47); 11 (36). As for the R_4-groups the highest frequencies concern 17 (54); 9 (35); 11 and 18 (32). The R_5-groups are dominated by substituents 113 (54); 221 (33). The top five scoring virtual hits namely analogs are: 2-8-9-8-218 (IC_{50}^{pre} = 0.21 nM), 2-8-9-8-219 (IC_{50}^{pre} = 0.31 nM), 2-8-10-18-108 (IC_{50}^{pre} = 0.58 nM), 2-8-9-8-121 (IC_{50}^{pre} = 0.65 nM) and 2-8-9-8-220 (IC_{50}^{pre} = 0.72 nM). They include the following substituents at R_1 position: 2: 5-(3-aminoprop-1-yn-1-yl)thiophen-2-yl (5), at R_3 position: 9 Me (4). Despite the hydrophobicity of the pocket exploited by the R_5-groups, their orientation to invest it seems to be dictated by other R-groups.

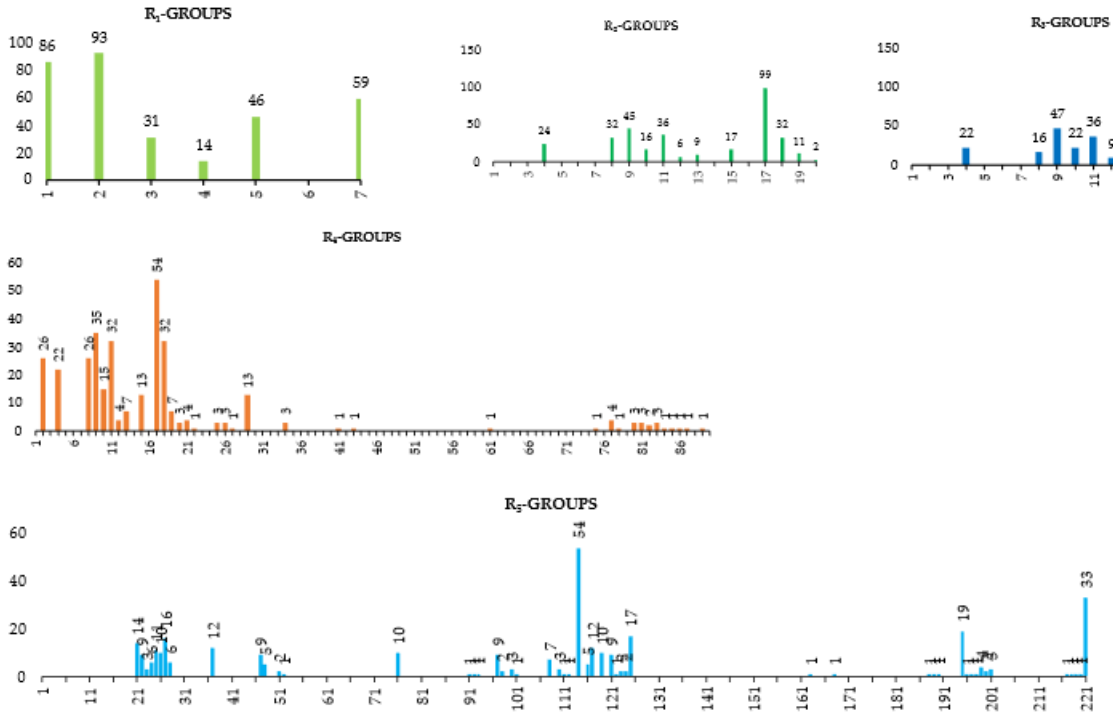

Figure 6. Histograms of frequency of occurrence of individual R-groups in the 329 best selected analogs mapping to four features of the PH4 pharmacophore hypothesis Hypo1 (for the structures of the fragments see Table 6); R_1 = 5-(3-aminoprop-1-yn-1-yl)thiophen-2-yl (2); R_2 = MeO (8); R_3 = Me (9), Cl (10); R_4 = MeO (8), NH2(18) and R_5 = ((3,3-diMebutyl)sulfonyl)carbamoyl (108), ((5-(Me-amino)pentyl)sulfonyl)carbamoyl (121),(R)-((5-(Etamino)hexyl)sulfonyl) carbamoyl(218),(R)-((5-(isopropylamino)hexyl)sulfonyl)carbamoyl(219),(3R,5R)-((5-(Etamino)-3-Mehexyl)sulfonyl) carbamoyl (220).

The substitutions in R_1 to R_5 positions of EHBs led to an overall increase of affinity of RdRp binding as exemplified by the inhibitory potencies of majority of new designed analogs. The best designed sulfonylbenzamide EHB 2-8-9-8-218 displays predicted half-minimal inhibitory concentration of $IC_{50}^{pre} = 0.21$ nM that is more than 100-times lower than that of the most active compound of the TS, namely the EHB1 with $IC_{50}^{exp} = 23$ nM, Figure 7, 8.

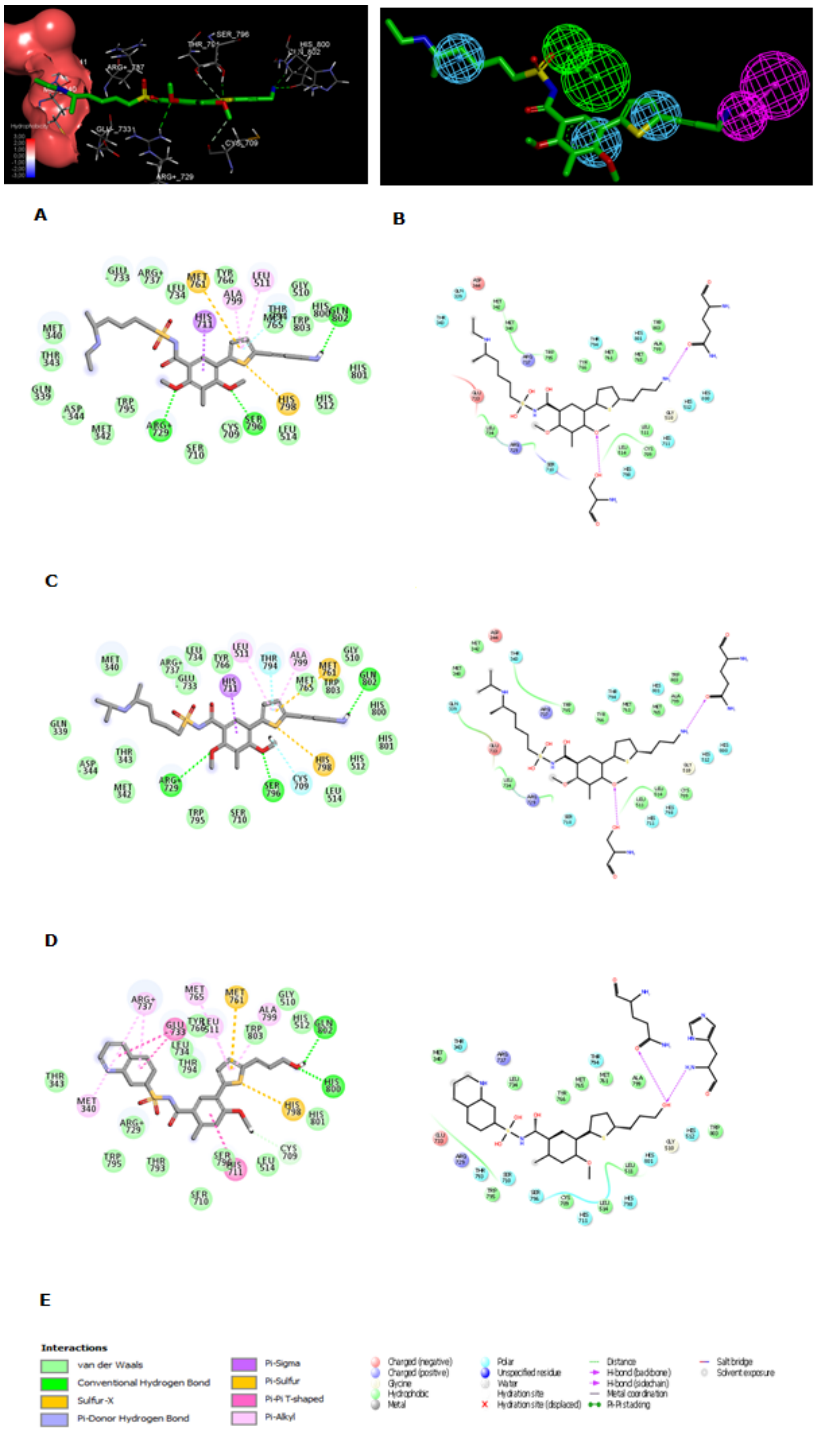

Figure 7. (A)-Close up of virtual hit 2-8-9-8-218, the most active designed EHB analog ($IC_{50}^{pre} = 0.21$ nM) at the active site of RdRp. Interacting residues are coloured by element. (B) - mapping of the EHB 2-8-9-8-218 to RdRp inhibition pharmacophore. (C) - 2D schematic interaction diagram of the EHB 2-8-9-8-218 at the active site of Denv RdRp. (D) - 2D schematic interaction diagram of the analog EHB2-8-9-8-219 ($IC_{50}^{pre} = 0.31$ nM) at the active site of Denv RdRp. (E) - 2D schematic interaction diagram of the ligand EHB1 at the active site of Denv RdRp.

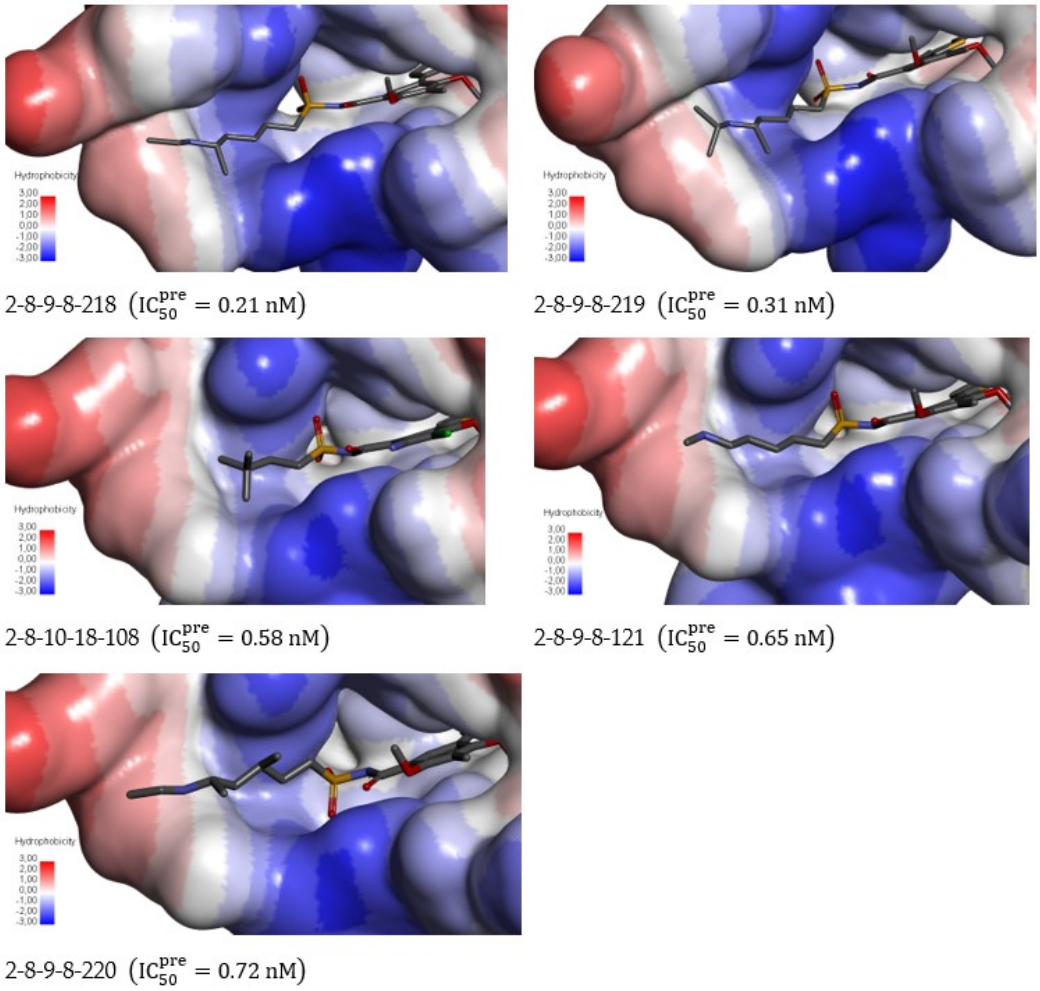

Figure 8. Surface of the active site of Denv RdRp with bound 5 best active designed EHB analogs. The binding site surface is colored according to residue hydrophobicity: red = hydrophobic, blue = hydrophilic and white = intermediate.

3.7 Pharmacokinetic Profile of Novel EHB Analogs

Many antivirals used in the treatment of viral infections exhibit a pharmacokinetic profile unsatisfactory with poor bioavailability and/or short half-life increasing the risk of ineffectiveness. Improving the pharmacokinetic characteristics of a drug requires improving its absorption profile. Improving the pharmacokinetic profile, i.e. increasing systemic exposure, increases the effectiveness of antiviral drugs, but also improves the quality of life of treated patients [24]. Although we do not have a specific antiviral against dengue, it seems advisable to compare, in Table 8, the properties linked to the ADME of our molecules with that of a known drug and sometimes used in the treatment of the dengue. Octanol-water partition coefficient, aqueous solubility, blood brain partition coefficient, Caco-2 cell permeability, serum protein binding, number of probable metabolic reactions and eighteen other descriptors related to absorption, the distribution, metabolism and excretion (ADME) of the new analogues were calculated by the QikProp program [25] based on the Jorgensen method [26,27]. Experimental data from over 710 compounds were used to produce regression equations correlating experimental and calculated descriptors resulting in an accurate prediction of the pharmacokinetic properties of the molecules. Since a value of less than 25% is considered poor, on the contrary, the 10 best predicted analogues show human oral absorption from the gastrointestinal tract (HOA) ranging from 48% to 83%, well above that of Ribavirin [28]. Drug likeness (#stars) - the number of property descriptors that fall outside the range of optimal values determined for 95%. The values of the best designed active EHBs are compared to those calculated for Ribavirin, Table 8. Most of our best designed analogs have #stars less than or equal to one. Thus, the designed EHBs exhibit a favorable pharmacokinetic profile.

Table 8. ADME-related properties of the best designed EHB analogs and known medicate either in clinical use to treat dengue or currently undergoing clinical testing computed by QikProp [26].

EHB Analogs [a]	# star[b]	M_W[c]	Smol[d]	Smol,hfo [c]	V_m [f]	RotB[g]	HBD[h]	HBA[i]	logPo/w[j]	logSwat[k]	logKHSA[l]	logB/B [m]	BIPcaco[n]	#meta[o]	IC_{50}^{pre} [p] (nM)	HOA[q]	%HOA[r]
2-9-17-81-125	1	464	797	222.8	1399	8	3	9.0	2.3	-4.9	0.23	-2.21	14.5	7	1.50	2	61
1-8-17-18-28	1	462	799	390.8	1406	9	3	7.4	3.5	-6.5	0.47	-2.36	98.3	4	1.91	1	83
1-13-10-15-125	2	482	794	345.5	1395	9	2	7.2	4.3	-6.8*	0.55	-1.65	302.9	4	1.31	1	96
2-8-10-18-108	0	484	811	364.9	1440	10	4	6.7	3.3	-5.6	0.55	-2.03	19.3	6	0.58	2	69
2-8-9-8-121	1	493	882	518.8	1555	13	4	9.0	2.6	-4.2	0.32	-1.83	8.0	8	0.65	2	58
7-9-9-2-76	1	485	797	259.9	1421	8	5	10.0	1.3	-4.4	0.02	-2.66	5.3	8	1.43	2	48
2-8-9-8-218	1	521	938	587.5	1665	14	4	9.0	3.3	-4.9	0.54	-1.81	10.5	8	0.21	2	52
2-8-9-8-219	2	535	959	614.2	1717	14	4	9.0	3.7	-5.3	0.67	-1.76	11.6	8	0.31	2	54
2-8-9-8-220	1	535	937	585.0	1698	14	4	9.0	3.5	-4.9	0.64	-1.78	9.9	8	0.72	2	52
Ribavirin [28]	1	244	435	106.8	728	5	5	12.3	-2.5*	-1.5	-0.95	-2.04	22.4	5	-	2	36

[a] Designed EHB analogs , Table 6 and known prophylactic treatment of dengue [□] [28]; [b] Drug likeness, number of property descriptors (24 out of the full list of 49 descriptors of QikProp, ver. 6.5, release 139) that fall outside of the range of values for 95% of known drugs; [c] Molar mass in [g.mol^{-1}] (range for 95% of drugs: 130–725 g.mol^{-1}) [26]; [d] Total solvent-accessible molecular surface, in [Å^2] (probe radius 1.4 Å) (range for 95% of drugs: 300–1000 Å^2); [e] Hydrophobic portion of the solvent-accessible molecular surface, in [Å^2] (probe radius 1.4 Å) (range for 95% of drugs: 0–750 Å^2); [f] Total volume of molecule enclosed by solvent-accessible molecular surface, in [Å^3] (probe radius 1.4 Å) (range for 95% of drugs: 500–2000 Å^3); [g] number of non-trivial (not CX3), non-hindered (not alkene, amide, small ring) rotatable bonds (range for 95% of drugs: 0–15); [h] estimated number of hydrogen bonds that would be donated by the solute to water molecules in an aqueous solution. Values are averages taken over several configurations, so they can assume non-integer values (range for 95% of drugs: 0.0–6.0); [i] Estimated number of hydrogen bonds that would be accepted by the solute from water molecules in an aqueous solution. Values are averages taken over several configurations, so they can assume non-integer values (range for 95% of drugs: 2.0–20.0); [j] Logarithm of partitioning coefficient between n-octanol and water phases (range for 95% of drugs: −2 to 6.5); [k] logarithm of predicted aqueous solubility, logS. S in [mol·dm^{-3}] is the concentration of the solute in a saturated solution that is in equilibrium with the crystalline solid (range for 95% of drugs: −6.0 to 0.5); [l] logarithm of predicted binding constant to human serum albumin (range for 95% of drugs: −1.5 to 1.5); [m] Logarithm of predicted brain/blood partition coefficient (range for 95% of drugs: −3.0 to 1.2); [n] Predicted apparent Caco-2 cell membrane permeability in Boehringer-Ingelheim scale in [nm.s^{-1}] (range for 95% of drugs: < 25 poor, > 500 nm.s^{-1} great); [o] Number of likely metabolic reactions (range for 95% of drugs: 1–8); [p] Predicted inhibition constants IC_{50}^{pre} of designed EHBx; [q] Human oral absorption (1 = low, 2 = medium, 3 = high); [r] Percentage of human oral absorption in gastrointestinal tract (<25% = poor, >80% = high); * star in any column indicates that the property descriptor value of the compound falls outside the range of values for 95% of known drugs.

4. DISCUSSIONS

A new approach to the inhibition of Denv RdRp replication by interaction with its specific site is reported by Fumiaki Yokokawa et *al* [16]. Their best designed EBHs are in hydrogen bond contact with Ser 796 by the sulfur of the thiophene ring, the sulfonylbenzamide part with Thr 794 and Trp 795, 3-hydroxyprop-1yn-1-yl in position 5 of the thiophene with His 800 and Gln 802, at the viral replication initiation loop and with Arg 729 of the palm subdomain. Our PH4 favors an HBD-Gln 802 which is confirmed by the complexation when replacing -OH by -NH_2, a strengthening of the ligand-Arg 729 bond the shortening of which fall from 2.96 Å for EBH3 to 2.76 – 2.90 Å for our top five novel analogues. This bond is made, for our new analogs, from the oxygen of the OMe in the R_4-group position instead of the oxygen of the sulfonyl. The bond with Ser796 already mentioned by other studies is preserved [8]. On the other hand, the decrease in the interaction energy between EHBs and Arg737 to the detriment of Thr794 which stabilizes the EHB-RdRp complex is also verified with our new analogues. Glu733 also plays a role in this stabilization of the complex. The investigation of the hydrophobic pocket by our best analogues confers them, in complex with RdRp, a great stability. The hydrophobic pocket's (Met340, Ala341 and Met342) filling, as a crucial requirement for affinity improvement, sheds light on the suitable substituents of R_5-groups. Among them bulky or long branched ones such as 218 and 219. As we can see on figure 9, the sum of interaction energy relative to hydrophobic pocket residues at the beginning of the residues' list (Met340, Ala341 and Met342) is -1.5 kcal/mol for EHB1 (the most active in the training set), -4.7 for 2-8-9-8-218 ($IC_{50}^{pre} = 0.21$ nM), -6.9 for 2-8-9-8-219 ($IC_{50}^{pre} = 0.31$ nM), -4.3 for 2-8-10-18-108 ($IC_{50}^{pre} = 0.58$ nM), -4.5 for 2-8-9-8-121 ($IC_{50}^{pre} = 0.65$ nM), -7.2 for 2-8-9-8-220 ($IC_{50}^{pre} = 0.72$ nM). They are four to five times lower than the interaction energy value for EHB1.

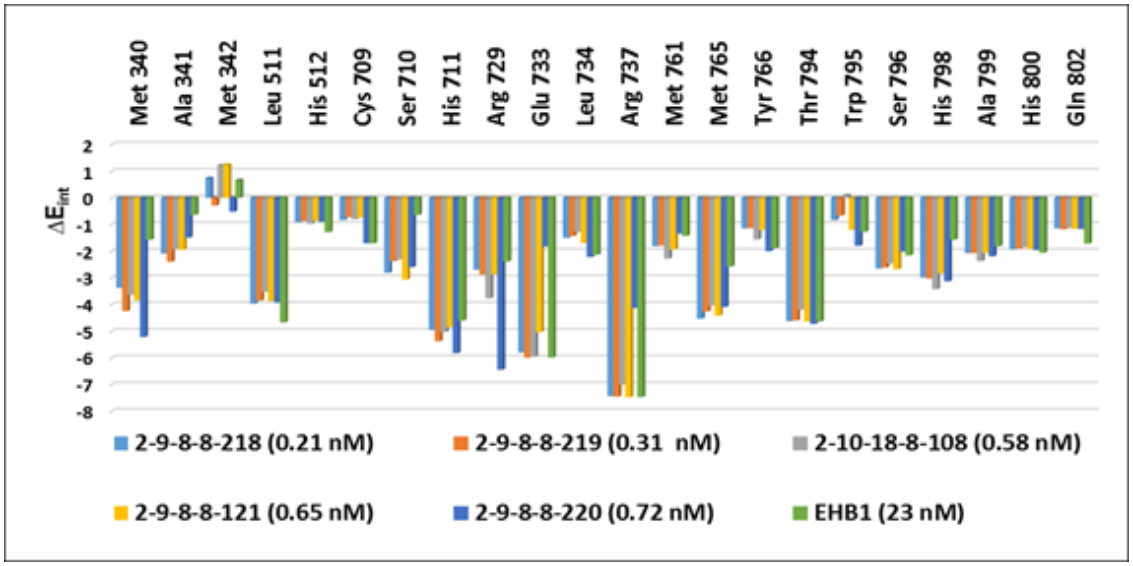

Figure 9. Molecular mechanics inter-molecular interaction energy E_{int} break-down to active site residue contributions in [kal.mol^{-1}]: designed best five novel EHB analogs (the color coding refers to ligands given in the legend).

5. CONCLUSION

In this work novel Denv RdRp inhibitors have been designed to reach the nanomolar inhibitory concentration range of the predicted IC_{50}^{pre} (Table 7, Figure 8). Even though these predicted inhibitory potencies may be somewhat too optimistic, they suggest that non-nucleosides Denv RdRp inhibitors more potent than the known TS and VS analogs [16] may exist. Our QSAR model provided bound RdRp inhibitor conformation, from which the decrease in the energy of the ligand-Arg737 interaction in favor of the energy of the ligand-Trh794 interaction as well as the decrease in Ligand-Met340 interaction energy at the active site confers stability to the enzyme-inhibitor complex which determines the predictive power of inhibition. Our new analogs identified by the 3D pharmacophore model QSAR with the singularity of the HBD ligand-Gln802 binding in the R_1 position and the hydrophobic clustering at residues Met340, Ala341 and Met342 exhibit predicted inhibitory potencies of RdRp: 2-8-9-8-218 ($IC_{50}^{pre} = 0.21$ nM), 2-8-9-8-219 ($IC_{50}^{pre} = 0.31$ nM), 2-8-10-18-108 ($IC_{50}^{pre} = 0.58$ nM), 2-8-9-8-121 ($IC_{50}^{pre} = 0.65$ nM) and 2 -8-9-8-220 ($IC_{50}^{pre} = 0.72$ nM) all with equally favorable pharmacokinetic profiles. This work, in addition to the new elements, has just reinforced that of Paul W. Smith et *al.* [16]. We therefore believe that these new analogs are worth synthesizing and evaluating.

Acknowledgement

The authors thank Eugene Megnassan for his helpful advice.

REFERENCES

[1] WHO. Dengue and severe dengue. (accessed on 2021/05/03/01:35:54) Available online: View Article

[2] WHO. Weekly epidemiological record; 34; 2015; pp. 421-432.

[3] Guzman, M.G.; Halstead, S.B.; Artsob, H.; Buchy, P.; Farrar, J.; Gubler, D.J.; Hunsperger, E.; Kroeger, A.; Margolis, H.S.; Martínez, E.; et al. Dengue: a continuing global threat. Nature Reviews Microbiology 2010, 8, S7-S16, doi:10.1038/nrmicro2460. PMid:21079655 View Article PubMed/NCBI

[4] Guo, J.-T.; Hayashi, J.; Seeger, C. West Nile Virus Inhibits the Signal Transduction Pathway of Alpha Interferon. Journal of Virology 2005, 79, 1343, doi:10.1128/JVI.79.3.1343-1350.2005. PMid:15650160 View Article PubMed/NCBI

[5] Koonin, E.V. Computer-assisted identification of a putative methyltransferase domain in NS5 protein of fla-viviruses and lambda 2 protein of reovirus. J Gen Virol 1993, 74 (Pt 4), 733-740, doi:10.1099/0022-1317-74-4-733. PMid:8385698 View Article PubMed/NCBI

[6] Yap, T.L.; Xu, T.; Chen, Y.-L.; Malet, H.; Egloff, M.-P.; Canard, B.; Vasudevan, S.G.; Lescar, J. Crystal Structure of the Dengue Virus RNA-Dependent RNA Polymerase Catalytic Domain at 1.85-Angstrom Resolution. Journal of Vi-rology 2007, 81, 4753, doi:10.1128/JVI.02283-06. PMid:17301146 View Article PubMed/NCBI

[7] Davidson, A.D. Chapter 2 New Insights into Flavivirus Nonstructural Protein 5. In Advances in Virus Research; Academic Press: 2009; Volume 74, pp. 41-101. 74002-3 View Article

[8] Anusuya, S.; Velmurugan, D.; Gromiha, M.M. Identification of dengue viral RNA-dependent RNA polymerase inhibitor using computational fragment-based approaches and molecular dynamics study. Journal of Biomolecular Structure and Dynamics 2016, 34, 1512

-1532, doi:10.1080/07391102.2015.1081620. PMid:26262439 View Article PubMed/NCBI

[9] Benmansour, F.; Eydoux, C.; Querat, G.; de Lamballerie, X.; Canard, B.; Alvarez, K.; Guillemot, J.-C.; Barral, K. Novel 2-phenyl-5-[(E)-2-(thiophen-2-yl) ethenyl]-1,3,4-oxadiazole and 3-phenyl-5-[(E)-2-(thiophen-2-yl)ethenyl]-1,2,4-oxadiazole derivatives as dengue virus inhibitors targeting NS5 polymerase. European Journal of Medicinal Chemistry 2016, 109, 146-156,. PMid:26774922 View Article PubMed/NCBI

[10] Manvar, D.; Küçükgüzel, İ.; Erensoy, G.; Tatar, E.; Deryabaşoğulları, G.; Reddy, H.; Talele, T.T.; Cevik, O.; Kaushik-Basu, N. Discovery of conjugated thiazolidinone-thiadiazole scaffold as anti-dengue virus polymerase inhibitors. Biochemical and Biophysical Research Communications 2016, 469, 743-747,. PMid:26697747 View Article PubMed/NCBI

[11] Nguyen, N.M.; Tran, C.N.B.; Phung, L.K.; Duong, K.T.H.; Huynh, H.l.A.; Farrar, J.; Nguyen, Q.T.H.; Tran, H.T.; Nguyen, C.V.V.; Merson, L.; et al. A Randomized, Double-Blind Placebo Controlled Trial of Balapiravir, a Polymer-ase Inhibitor, in Adult Dengue Patients. The Journal of Infectious Diseases 2013, 207, 1442-1450, doi:10.1093/infdis/jis470. PMid:22807519 View Article PubMed/NCBI

[12] Nitsche, C.; Schreier, V.N.; Behnam, M.A.M.; Kumar, A.; Bartenschlager, R.; Klein, C.D. Thiazolidinone-Peptide Hybrids as Dengue Virus Protease Inhibitors with Antiviral Activity in Cell Culture. Journal of Medicinal Chemistry 2013, 56, 8389-8403, doi:10.1021/jm400828u. PMid:24083834 View Article PubMed/NCBI

[13] Vincetti, P.; Caporuscio, F.; Kaptein, S.; Gioiello, A.; Mancino, V.; Suzuki, Y.; Yamamoto, N.; Crespan, E.; Lossani, A.; Maga, G.; et al. Discovery of Multitarget Antivirals Acting on Both the Dengue Virus NS5-NS3 Interaction and the Host Src/Fyn Kinases. Journal of Medicinal Chemistry 2015, 58, 4964-4975, doi:10.1021/acs.jmedchem.5b00108. PMid:26039671 View Article PubMed/NCBI

[14] Xu, H.-T.; Colby-Germinario, S.P.; Hassounah, S.; Quashie, P.K.; Han, Y.; Oliveira, M.; Stranix, B.R.; Wainberg, M.A. Identification of a Pyridoxine-Derived Small-Molecule Inhibitor Targeting Dengue Virus RNA-Dependent RNA Polymerase. Antimicrob Agents Chemother 2015, 60, 600-608, doi:10.1128/AAC.02203-15. PMid:26574011 View Article PubMed/NCBI

[15] Yin, Z.; Chen, Y.-L.; Schul, W.; Wang, Q.-Y.; Gu, F.; Duraiswamy, J.; Kondreddi, R.R.; Niyomrattanakit, P.; Laksh-minarayana, S.B.; Goh, A.; et al. An adenosine nucleoside inhibitor of dengue virus. Proceedings of the National Academy of Sciences 2009, 106, 20435, doi:10.1073/pnas.0907010106. PMid:19918064 View Article PubMed/NCBI

[16] Yokokawa, F.; Nilar, S.; Noble, C.G.; Lim, S.P.; Rao, R.; Tania, S.; Wang, G.; Lee, G.; Hunziker, J.; Karuna, R.; et al. Discovery of Potent Non-Nucleoside Inhibitors of Dengue Viral RNA-Dependent RNA Polymerase from a Fragment Hit Using Structure-Based Drug Design. Journal of Medicinal Chemistry 2016, 59, 3935-3952, doi:10.1021/acs.jmedchem.6b00143. PMid:26984786 View Article PubMed/NCBI

[17] Zhao, Z.; Bourne, P.E. Structural Insights into the Binding Modes of Viral RNA-Dependent RNA Polymerases Using a Function-Site Interaction Fingerprint Method for RNA Virus Drug Discovery. Journal of Proteome Research 2020, 19, 4698-4705, doi:10.1021/acs.jproteome.0c00623. PMid:32946692 View Article PubMed/NCBI

[18] Potisopon, S.; Priet, S.; Selisko, B.; Canard, B. Comparison of dengue virus and HCV: from impact on global health to their RNA-dependent RNA polymerases. Future Virology 2014, 9, 53-67, doi:10.2217/fvl.13.121. View Article

[19] Zhao, Y.; Soh, T.S.; Zheng, J.; Chan, K.W.K.; Phoo, W.W.; Lee, C.C.; Tay, M.Y.F.; Swaminathan, K.; Cornvik, T.C.; Lim, S.P.; et al. A Crystal Structure of the Dengue Virus NS5 Protein Reveals a Novel Inter-domain Interface Essen-tial for Protein Flexibility and Virus Replication. PLOS Pathogens 2015, 11, e1004682, doi:10.1371/journal.ppat.1004682. PMid:25775415 View Article PubMed/NCBI

[20] Allangba, K.N.G.P.G.; Keita, M.; Kre N'Guessan, R.; Megnassan, E.; Frecer, V.; Miertus, S. Virtual design of novel Plasmodium falciparum cysteine protease falcipain-2 hybrid lactone-chalcone and isatin-chalcone inhibitors prob-ing the S2 active site pocket. J Enzyme Inhib Med Chem 2019, 34, 547-561, doi:10.1080/14756366.2018.1564288. PMid:30696325 View Article PubMed/NCBI

[21] Kouassi, A.F.; Kone, M.; Keita, M.; Esmel, A.; Megnassan, E.; N'Guessan, Y.T.; Frecer, V.; Miertus, S. Comput-er-Aided Design of Orally Bioavailable Pyrrolidine Carboxamide Inhibitors of Enoyl-Acyl Carrier Protein Reductase of Mycobacterium tuberculosis with Favorable Pharmacokinetic Profiles. International Journal of Molecular Sciences 2015, 16, doi:10.3390/ijms161226196. PMid:26703572 View Article PubMed/NCBI

[22] N'Guessan, H.; Megnassan, E. In silico Design of Phosphonic Arginine and Hydroxamic Acid Inhibitors of Plas-modium falciparum M17 Leucyl Aminopeptidase with Favorable Pharmacokinetic Profile. Journal of Drug Design and Medicinal Chemistry 2017, 3, 86-113, doi:10.11648/j.jddmc.20170306.13 View Article

[23] Lipinski, C.A.; Lombardo, F.; Dominy, B.W.; Feeney, P.J. Experimental and computational approaches to estimate solubility and permeability in drug discovery and development settings1PII of original article: S0169-409X(96)00423-1. The article was originally published in Advanced Drug Delivery Reviews 23 (1997) 3-25.1. Advanced Drug Delivery Reviews 2001, 46, 3-26. 00423-1 View Article

[24] Paci-Bonaventure, S.; Le Tiec, C.; Taburet, A.M. Pharmacochemical tools: a new approach to improve pharmaco-kineticprofile of new antiviral drugs. La Lettre de l'infectiologue 2004, 19, 113-117.

[25] Schrödinger QikProp 6.5 (rel139), Schrödinger LLC: New York, NY, 2019.

[26] Jorgensen, W.L.; Duffy, E.M. Prediction of drug solubility from Monte Carlo simulations. Bioorganic & Medicinal Chemistry Letters 2000, 10, 1155-1158.

00172-4 View Article
[27] Jorgensen, W.L.; Duffy, E.M. Prediction of drug solubility from structure. Advanced Drug Delivery Reviews 2002, 54, 355-366. 00008-X View Article
[28] Malinoski, F.J.; Hasty, S.E.; Ussery, M.A.; Dalrymple, J.M. Prophylactic ribavirin treatment of dengue type 1 infec-tion in rhesus monkeys. Antiviral Research 1990, 13, 139-149. 90029-7 View Article
[29] Berman, H.M.; Westbrook, J.; Feng, Z.; Gilliland, G.; Bhat, T.N.; Weissig, H.; Shindyalov, I.N.; Bourne, P.E. The Protein Data Bank. Nucleic Acids Research 2000, 28, 235-242, doi:10.1093/nar/28.1.235. PMid:10592235 View Article PubMed/NCBI
[30] Accelrys Inc. Insight-II and Discover Molecular Modeling and Simulation Package, Release 2005; Accelrys Inc.: San Diego, CA, USA, 2005.
[31] Dali, B.; Keita, M.; Megnassan, E.; Frecer, V.; Miertus, S. Insight into Selectivity of Peptidomimetic Inhibitors with Modified Statine Core for Plasmepsin II of Plasmodium falciparum over Human Cathepsin D. Chemical Biology & Drug Design 2012, 79, 411-430. PMid:22129033 View Article PubMed/NCBI
[32] e-Eknamkul, W.; Umehara, K.; Monthakantirat, O.; Toth, R.; Frecer, V.; Knapic, L.; Braiuca, P.; Noguchi, H.; Miertus, S. QSAR study of natural estrogen-like isoflavonoids and diphenolics from Thai medicinal plants. Journal of Molecular Graphics and Modelling 2011, 29, 784-794. PMid:21334935 View Article PubMed/NCBI
[33] Esmel, A.; Keita, M.; Megnassan, E.; Toï, B.; Frecer, V.; Miertus, S. Insight into binding mode of nitrile inhibitors of Plasmodium falciparum Falcipain-3, QSAR and Pharmacophore models, virtual design of new analogues with fa-vorable pharmacokinetic profiles. Journal of Computational Chemistry & Molecular Modeling 2017, 2, 103-124. View Article
[34] Frecer, V.; Berti, F.; Benedetti, F.; Miertus, S. Design of peptidomimetic inhibitors of aspartic protease of HIV-1 containing -PheΨPro- core and displaying favourable ADME-related properties. Journal of Molecular Graphics and Modelling 2008, 27, 376-387. PMid:18678515 View Article PubMed/NCBI
[35] Frecer, V.; Burello, E.; Miertus, S. Combinatorial design of nonsymmetrical cyclic urea inhibitors of aspartic pro-tease of HIV-1. Bioorganic & Medicinal Chemistry 2005, 13, 5492-5501. PMid:16054372 View Article PubMed/NCBI
[36] Frecer, V.; Megnassan, E.; Miertus, S. Design and in silico screening of combinatorial library of antimalarial ana-logs of triclosan inhibiting Plasmodium falciparum enoyl-acyl carrier protein reductase. European Journal of Medici-nal Chemistry 2009, 44, 3009-3019. PMid:19217192 View Article PubMed/NCBI
[37] Frecer, V.; Miertus, S.; Tossi, A.; Romeo, D. Rational design of inhibitors for drug resistant HIV-1 aspartic protease mutants. Drug design and discovery 1998, 15, 211-231.
[38] Megnassan, E.; Keita, M.; Bieri, C.; Esmel, A.; Frecer, V.; Miertus, S. Design of Novel Dihydroxynaphthoic Acid Inhibitors of Plasmodium Falciparum Lactate Dehydrogenase. Medicinal Chemistry 2012, 8, 970-984, doi. PMid:22741776 View Article PubMed/NCBI
[39] Owono, L.C.; Keita, M.; Megnassan, E.; Frecer, V.; Miertus, S. Design of Thymidine Analogues Targeting Thymidi-late Kinase of *Mycobacterium tuberculosis*. Tuberculosis Research and Treatment 2013, 2013, 670836, doi:10.1155/2013/670836. PMid:23634301 View Article PubMed/NCBI
[40] Owono Owono, L.C.; Ntie-Kang, F.; Keita, M.; Megnassan, E.; Frecer, V.; Miertus, S. Virtually Designed Triclo-san-Based Inhibitors of Enoyl-Acyl Carrier Protein Reductase of Mycobacterium tuberculosis and of Plasmodium falciparum. Molecular Informatics 2015, 34, 292-307, doi:10.1002/minf.201400141. PMid:27490275 View Article PubMed/NCBI
[41] Gilson, M.K.; Honig, B. The inclusion of electrostatic hydration energies in molecular mechanics calculations. Journal of Computer-Aided Molecular Design 1991, 5, 5-20, doi:10.1007/BF00173467. PMid:2072125 View Article PubMed/NCBI
[42] Rocchia, W.; Sridharan, S.; Nicholls, A.; Alexov, E.; Chiabrera, A.; Honig, B. Rapid grid-based construction of the molecular surface and the use of induced surface charge to calculate reaction field energies: Applications to the molecular systems and geometric objects. Journal of Computational Chemistry 2002, 23, 128-137. PMid:11913378 View Article PubMed/NCBI
[43] Li, H.; Sutter, J.; Hoffmann, R. HypoGen: an automated system for generating 3D predictive pharmacophore models. Pharmacophore perception, development, and use in drug design 2000, 2, 171.